Bachelor Thesis

DYNAMICS AND CONTROL OF ACROBATIC KITES

Author:
Pablo Manuel Muñoz de la Flor

Director:
Gonzalo Sánchez Arriaga

September 2016

Glory is only achieved by fighting

ad augusta per angusta

Contents

List of Figures

List of Tables

List of symbols

t (s)	Time
t^* (s)	Characteristic time
g (m/s^2)	Gravitational acceleration
L_0 (m)	Initial length of tethers
B (m)	Kite span
C (m)	Kite chord
H (m)	Kite height
X_A (m)	Attached point x-coordinate
Y_A (m)	Attached point y-coordinate
Z_A (m)	Attached point z-coordinate
λ (m)	Kite elliptical cross-section length
S (m^2)	Kite surface
M (kg)	Kite mass
I_{xx}	Dimensionless inertia tensor x-component
I_{yy}	Dimensionless inertia tensor y-component
I_{zz}	Dimensionless inertia tensor z-component
ρ (kg/m^3)	Air density
σ (kg/m^2)	Kite surface mass distribution
$L_{A_\pm}$ (m)	Time dependent wires length
P (rad/s)	Angular velocity x-component
Q (rad/s)	Angular velocity y-component
R (rad/s)	Angular velocity z-component
V_A (m/s)	Aerodynamic velocity
V_W (m/s)	Wind velocity
V_T (m/s)	Reference velocity
V^* (m/s)	Characteristic velocity
α	Angle of attack
β	Sideslip angle
e_k	Kinetic energy
u_p	Potential energy
c_{x_0}, c_{z_0} and c_{m_0}	Aerodynamic coefficients
c_{x_α}, c_{y_β} and c_{z_α}	Aerodynamic force coefficients
c_{l_β}, $c_{l_{p'}}$, c_{m_α}, $c_{m_{q'}}$, c_{n_β} and $c_{n_{r'}}$	Aerodynamic moment coefficients

1 Introduction

1.1 State of art

Energy is a need. Nowadays, energy is needed for a lot of common daily affairs. Energy generation was possible in the past thanks to fossil sources, like carbon. Today, these fossil resources still play a huge role in energy production, but human has realized that these means are not infinite.

The solution for this problem is the so-called renewable energy sources as sun, wind, water, biomass... Sun is used for obtaining energy by photovoltaic panels or for heating water at home, sun can radiate more energy that the one used by human since the beginning of time in only one second , in [1] more information can be found. The water of the sea is used to produce energy due to the so-called tidal energy and also in reservoir to produce energy too, it must be moved for energy production; this kinetic energy is transformed into power by moving turbines; there are projects for develop this kind of energy production as [2]. Biomass is all organic material that comes from plants; energy is stored in the chemical bonds of this organic material; according to [3], biomass produces between 10 and 14 % of the world energy.

Finally, wind is used in different ways; in figure 1 below, there are several concepts explained. Wind is very powerful, it contains energy equivalent to 100 times the one used by human civilization. In the black square of figure 1, the different types of Jet Stream that are in the earth are shown. These jet streams are composed by high-speed wind. This wind, usually is availed for energy production by windmill fields or wind-farms. These kind of system is enormous and it does not take advantage of wind in the best way because its height is not enough to reach the altitude at which wind is very strong. For solving this problem, a new solution came up; simpler systems that can reach very high altitudes, kites.

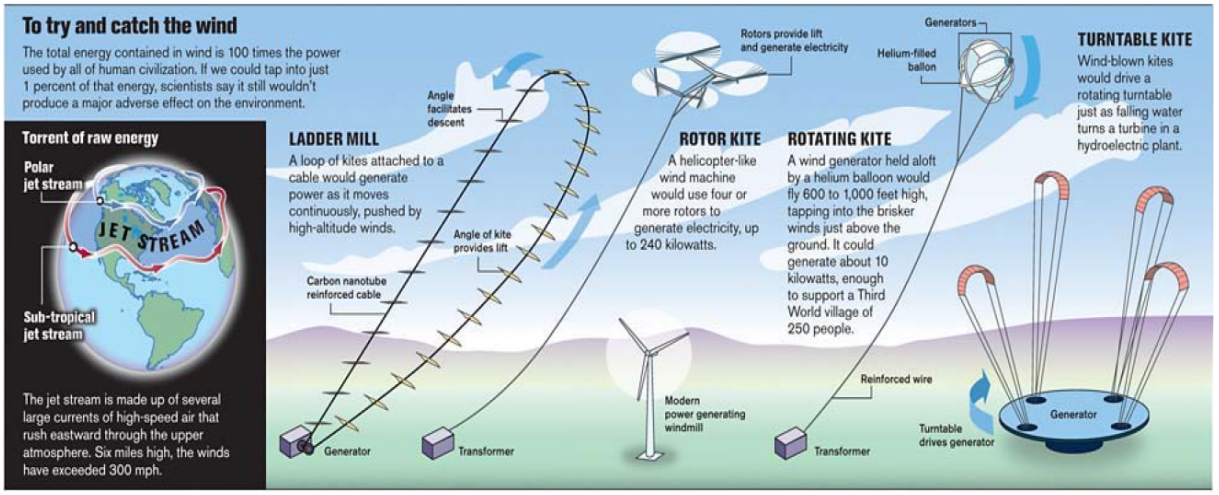

Figure 1: Principal kite power generation types, figure from [4]

In the figure 1, four types of energy generation by kites can be seen, each one with different functionality. There are two main groups in these kind of systems, FlyGen and GroundGen, the first contains systems that produced energy on-board transmitting it to ground. In the other hand, GroundGen systems produce energy on ground thanks to the motion of the system. In next sections are explained carefully the classification of energy generation and the different types of systems introduced in previous figure 1.

1.1.1 Classification of wind systems with kites

Generation of energy by means of kites is a development field with a lot of investigation lines. The more investigated case is the kite attach to ground by one line, as study in [5]. Kites with two lines have not been widely investigated, and then the aim of this Bachelor Thesis is to research the energy production of this kind of tethered aircraft.

The more used methods are High Altitude Wind Production Systems (HAWPS). Archer & Caldeira [2009] analysed 28 years of wind statistics at altitudes between 500 meters and 12000 meters and established that there is an enormous amount of energy in the winds at high altitude [Jeroen]. This is why HAWPS are more used, because the energy production is bigger. There are different types of energy production, according to [12], three varieties are the principal ones (containing each of them different methods):

- FlyGen
- GroundGen
- Propulsion of Vehicles

FlyGen are systems that produce energy in the vehicle and transmit it along the wire to a transformer placed in the ground station. GroundGen systems generate energy on ground; they can generate energy from the motion of the vehicle in the ground station at which there is a generator. Finally, the last type is not directly an energy production method, it substitutes the energy needed to move a vehicle (usually boats) by the traction made by a kite.

The following points are going to introduce the principal HAWPS, shown in picture 1.

1.1.1.1 The 'Pumping' Laddermill or Kite Reel

This is a GroundGen system that consist in a group of joined kites and was originally developed by David Lang. Kites are joined as shown in left part of figure 2. What also shows this part of the figure is the control system attached to kites. This control system allows to modify the angle of attack of all kites and change between reel-out and back motion. Both motions, when wire is released and when it is collected, make the generator work and produce energy. During the reel-out or power stroke, the kite is at a high angle of attack and pulls at maximum load [4]. For the reeled back, the angle of attack is lowered, collecting the wire for beginning again the cycle. The maximum power is obtained during the reel-out because a higher force is produced.

Electrical and mechanical components needed are simple and they are content in the ground station, which can be seen in the right part of the figure below obtained from [4]. This ground station content the generator driven by wires' tension and the transformer needed for this power generation.

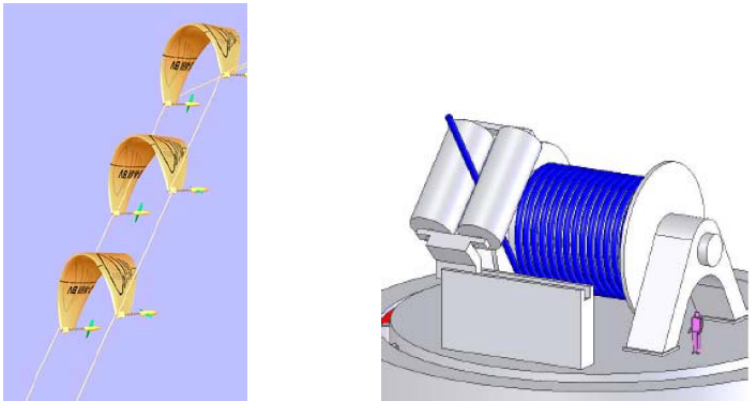

Figure 2: Control system and ground station, figure from [4]

This David Lang's system, which research was performed by Dr. Wubbo Ockels, a former NASA astronaut, at Delft University (Netherlands), can produce more energy by increasing kite area and by stacking kites. This energy generator is considered to be the most likely to succeed out of the many high altitude energy concepts that have been proposed due to its simple nature and higher technology readiness level [4].

According to [6], these kites are not flexible, they behave as rigid solids, the same as the kite that has been modelled in the present Bachelor Thesis. Five kites acquiring this configuration allow to generate 2 kWh every four minutes, reaching the same amount of power that a windmill with same swept area as [6] calculations show.

1.1.1.2 Rotor Kite

This system is a FlyGen one which has the concept of the gyrocopter with 4 rotors. The name of it is Flying Electric Generator (FEG) and it flies following the same principle than kites. These large rotors, moved by wind that pass through them, produce lift that allows to fly at high altitudes and turn the generators placed on the structure (fly generator -FlyGen- concept).

Generator is on-board and the obtained power is transferred to the transformer, which is placed on ground, by the tethers; they are insulated and made of aluminium conductors, they also are wound with strong Kevlar-family cords. The conductor weight is a critical issue because of the power loss and heat generation. As [7] informs, rotors have their open faces at an angle up to 50º for taking in advance the wind at they fly; they fly in regions at which there is powerful and persistent wind. The angle mentioned can be related to the angle of attack that usual kites acquire, being 50º the maximum, so the stall angle, at which rotor kite produces the maximum lift, so the maximum power.

This kind of systems can also have more than four rotors, which obviously will produce more power. In figure 3 a system with four rotors is shown; it is also observable the path of the air through rotors. These kites compose wind farms in US, Netherlands and Canada, where they fly at 9 kilometres in the sky for reaching the jet stream.

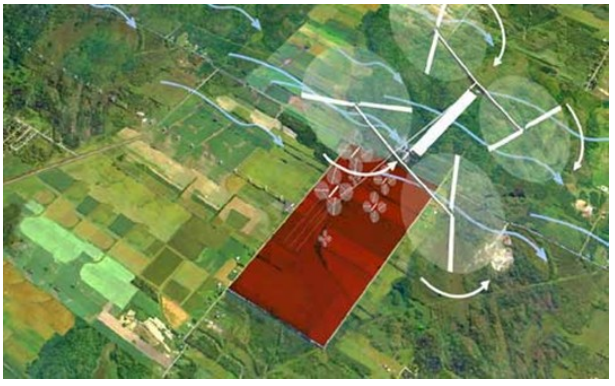

Figure 3: Four rotor demonstration craft, figure from [8]

1.1.1.3 Rotating kite

This system follows a principle similar to the one explained in rotor kite, so it is also a FlyGen system. This project developed by Magenn consists on a balloon structure filled by helium which contains a generator inside it. The generator is driven by the rotation of the system; and this rotation is caused by the wind and the external shape of the structure. The shape is like a pinwheel if looked in profile; it has sails with wind hits against making the system rotate. This system usually flies at altitudes between 200 m and 350 m. It rotates around a horizontal axis connected to a generator whose size is limited by the balloon because of it is content inside.

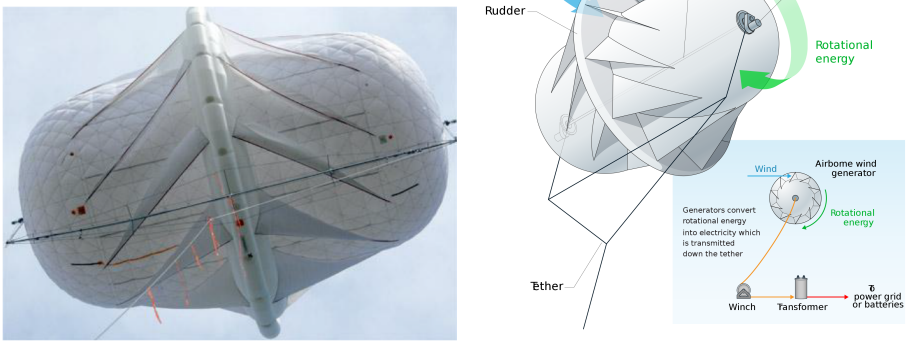

(a) Air Rotor System (b) Working principle

Figure 4: Magenn project, figures from [7]

At figure 4 the system can be observed. At figure 4(a), the balloon, tether and attachment points can be seen. The same at figure 4(b) which the system is schematically explained showing the position of the sails and their effect on the rotation of the system. What is not showed in figure and it is important to realize is the issue of lift. The system needs lift to keep itself flying apart from the action that the helium produces for keeping the balloon flying. The additional produced lift is provided by 'Magnus effect' which states, as [7] introduces, that a rotating object in the air generates lift for itself.

As in rotor kite, power is generated on-board and it must be transmitted to ground where the transformer is placed. Tether, also as in previous system, conduces the power to ground. Apart from the cost of the system, tether has also a significant cost as it must be made of a material that conduces power and it must also be insulated for not to loss energy during the transmission. Tether costs are studied to be reduced.

1.1.1.4 Turntable kite

This system changes the concept of the ones introduced before. This GroundGen system is composed by different groups of kites attached to a structure which rotates thanks to the traction done by these groups of kites. The generator is placed inside this structure. Each group of kites acquires a configuration similar to Laddermill one. For benefit of wind, kites fly between 800 meters and 2000 meters of altitude.

This kind of system is developed by KiteGen, a project which was born in Italy by means of Dr. Massimo Ippolito. This project is named carousel configuration and includes in each arm, at which groups of kites are attached, a KSU (Kite Steering Unit). The purpose is to maximize the exerted torque before transmitting the motion to the generator; this is made, as explained in [9], by the controller of each kite.

At figure 5(a) all groups of kites can be seen attached to the different arms of the structure. This multiple kite configuration similar to Laddermill requires automatic control technology, which is currently used in single kites configuration.

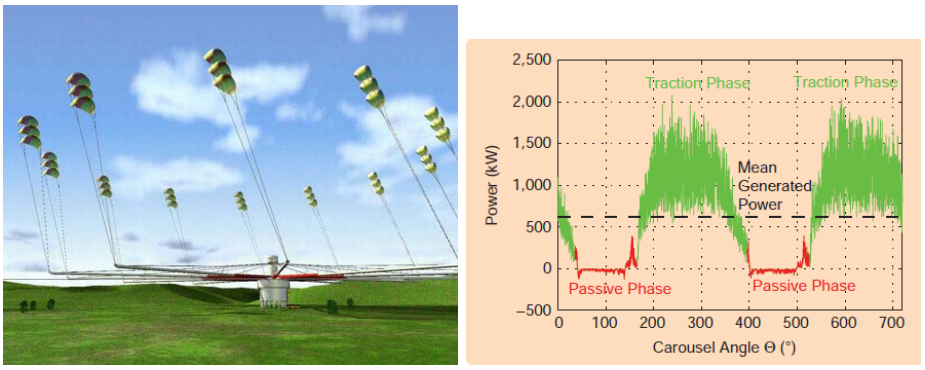

(a) Carousel configuration, figure from [4] (b) Power generated, figure from [9]

Figure 5: Carousel configuration, a KiteGen project

In the other hand, figure 5(b) shows the power generated by this system versus the angle of the system. It is clearly showed that during traction phase a higher power is obtained. According to [9], the mean value of the power generated during the two traction phases is 621 kW and the generated energy per cycle is 234 MJ.

1.1.1.5 Propulsion of vehicles

The last type of energy production is not directly a production of energy system, but a substitution of power use. This method allows to save fuel thanks to the traction force produced by kites. This type of solution let save fuel, so, it saves money. It is very important nowadays, because all manufacturers of not only ships, but also cars, aircraft and all vehicles powered by fuel, focus on the problem of saving fuel for being more economically competitive.

Another worrying problem that must be taken into account is the pollution. All vehicles that consume fuel, due to the combustion, emit harmful gasses for human and for nature. This gasses are responsible specially of the greenhouse. Currently, so many manufacturers, impulsed by governments, are trying to reduce emissions.

Actually there are businesses and work groups that study to develop traction vehicles. This is very important to reduce the fuel consumption in order to reduce the CO_2 emissions which are the 3% of the total emissions of the world, according to [10]. There are cargo ships testing this systems and they can save between 10 and 30 % of fuel.

At figure 6(a) an example of a cargo ship propelled by this system is shown. This system is installed by SkySails, a business dedicated to maritime green energy. This company is a pioneer introducing this system in cargo ships. The system consists on a towing kite with rope, a launch and recovery system, and a control system for automated operation.

(a) Skysails example, figure from [10]

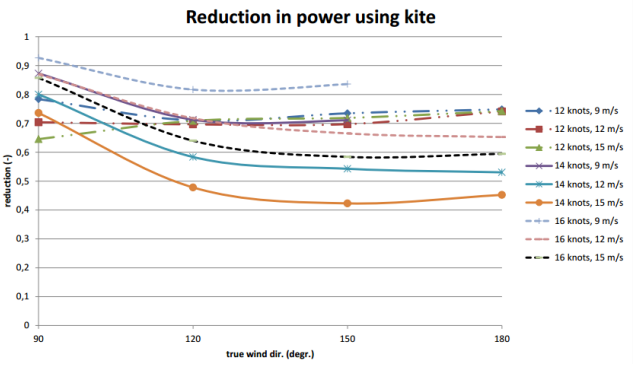

(b) Reduction in power using this system, figure from [11]

Figure 6: Skysails propulsion of vehicles

Figure 6(b) shows a graph with different results of simulations for obtaining the reduction in power of ships versus the direction of the wind. The are several simulations covering combinations of velocities of ship (in knots) and wind (in m/s). Kite propulsion is very effective, but its main drawback for the installation is that, as [11] calculate, the payback time is high.

1.1.2 Principal characteristics of FlyGen and GroundGen

1.1.2.1 FlyGen

As explained in previous cases of FlyGen systems, they are lighter than air and they include the generator on-board moved thanks to wind and the structure architecture of the system. Another principal characteristic of this kind of generator vehicles is that generated power is transmitted through the tether.

- The main drawback of these systems is the need of reducing the size of the turbines because of the low weight of the system, so it forces to operate at high velocities.
- In the other hand, the main advantage is that this is the HAWP system with greatest power peak [12], which implies a very attractive issue for public and investors.

Another example of this kind of systems is the Makani prototype. Makani is a project of Google which is able to generate 600 kW. The prototype has 8 DC motors and it operates at altitudes between 140 meters and 310 meters with a cycling radius of 145 meters, as [13] explains. This project is more expensive than other ones because of its complex technology. At figure 7 prototype can be seen flying; it can be also appreciated motors and wires.

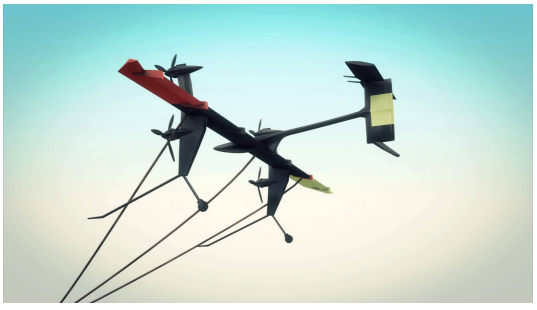

Figure 7: Example of a rigid kite with generators, figure from [14]

1.1.2.2 GroundGen

These other kind of generator systems have a principal characteristic which is that the generator is on ground instead of on-board like in FlyGen systems. This issue allows to eliminate the conductor wire, so the tether is cheaper than the one used in FlyGen systems.

The generation of energy is produced in different cycles which have 2 stages each one (reel-out and reel-back). This process is known as energy pumping, which have different options, but the most used one is the case at which an eight (8) manoeuvre is described in a curved trajectory in form of ∞ to maximize the time at which the tension force is available. In figure 8 the operating schema with both stages can be seen.

- The most important advantage is the capacity factor. Capacity factor is the one for which it is necessary to reduce the capacity of generation in order to take into account the time at which the system is not producing energy (when there is not wind). To clarify with an example, a windfarm has this factor near the 30 % and a typical HAWP system can be near to 52 % because of the high-altitude wind, which are more frequent and constant. In other words, an HAWP system produces a little bit less energy, but it operates for longer periods of time, offering more energy.
  - The second main advantage is that the presence of wind at high altitude is more frequent than at low altitudes. This means that it is easy to find places to locate windfarms benefiting the opportunity of generating energy in places where previously there were not means to take the advantage of it. This means that these systems are not going to substitute the current ones, they can obtain more energy using new locations.
  - Another important advantage is that the costs of installation and materials is low in comparison with FlyGen systems. These systems can also be transported easily.
- The principal drawback is that the power produced by these kind of systems is not as high as on FlyGen systems. The peak power in FlyGen is so higher than GroundGen one.

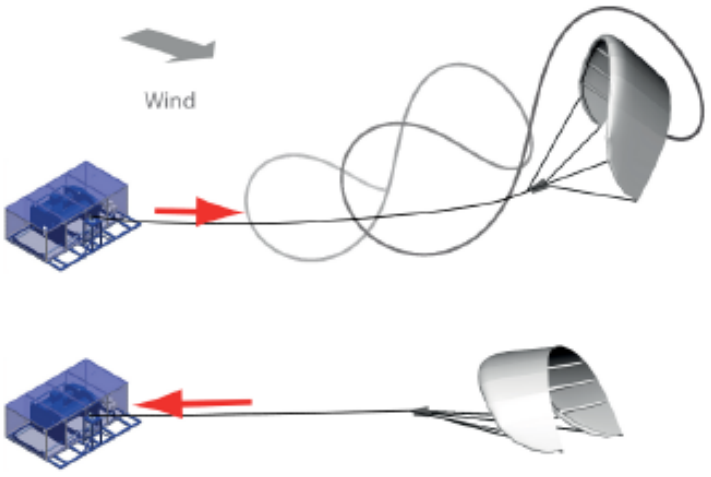

Figure 8: Operating Schema, figure from [5]

1.1.3 FlyGen vs GroundGen

In conclusion of the previous sections, Groundgen systems cannot compite with Flygen ones in terms of power. In comparison with conventional turbines, the competition depends on more factors, like the presence of high velocity wind at high altitude.

Definitively, GroundGen systems are cheaper and they can be easily transported and FlyGen systems produce a larger amount of power but with a more complex technology, supposing, obviously, a higher production price. So, for installing a kite generation system, a study in terms of money and needs must be done before choosing one system or the other.

1.1.4 Limits of HAWP systems

HAWP system have a power production limit, which can be found according to Power Limit of Airborne Wind Energy Theorem which reads [12]:

Let us regard a wing with area A and aerodynamic coefficients C_L and C_D that is moved in a wind field of constant wind speed v_w with air density ρ. When the wing's motion through this wind field is not only influenced by its intrinsic lift and drag, but also by additional drag forces, such as an on-board turbine with corresponding drag coefficient $C_{D;power}$ and by non-aerodynamic forces, such as a tether, then the total usable power P that can be harvested from the wind using these extra forces is limited by:

$$P \leq \frac{2}{27}\rho A V_w^2 C_R \left(\frac{C_R}{C_D}\right)^2; \quad C_R = C_L\sqrt{1+\left(\frac{C_D + C_{D,pow}}{C_L}\right)^2}$$

Where:

- P is the maximum limit power that can be extracted from the system
- ρ is the density of the air
- A is the surface of the kite
- V_w is the velocity of the wind
- C_D is the coefficient of the Drag Aerodynamic force
- C_L is the coefficient of the Lift Aerodynamic forc
- $C_{D,pow}$ is the factor of resistance introduced by a shipped generator

This limit of power can be only achieved if total aerodynamic force is aligned with wind, if the wing drag is the only loss, and the airspeed of the wing is made equal to:

$$V_a = \frac{2C_R}{3C_D}V_w$$

This limit explains why investors have more interest in Flygen systems with rigid wing: it is possible to obtain an increase in the power, adding systems which generate during flight ($C_{D,pow}$ factor) and improving the aerodynamic efficiency, which is easier to do in rigid wing than in flexible ones [5].

It is also interesting to compare the useful power P given by a wing with area A with the wind power P_{area} that flows through a cross sectional area of the same size. They are compared via the Power Harvesting Factor, ζ:

$$\zeta = \frac{P}{P_{area}} = \frac{P}{\frac{1}{2}\rho A V_w^3}$$

Where:

- P is the power extracted from the system
- P_{area} is the power that can be extracted from a tube of flow of surface A
- A is the wing surface

Following the previous introduced theorem, an upper limit of the Harvesting Factor can be determined, reading:

$$\zeta \leq \zeta_{max} = \frac{4}{27} C_R \left(\frac{C_R}{C_D} \right)^2$$

According to [12] the maximum theoretical value of the factor for generation with kites is equal to 30, but actually, the maximum value reached is 8, achieved by Makani. The maximum obtained in non-rigid kites is 4, lower than the aero-generators.

1.1.5 Related studies

1.1.5.1 Goela

One of the first studies about power generation by kites was made by Dr. Goela. He performed in 1983 an analysis of the steady state motion of the kite during both stages of its motion, ascent and descent. As [15] explains, he focused on forces done by kite and acting on kite caused by kite motion. He also studied factors acting on kite and time between descent and ascent phases.

Goela's team also studied the kite design; several different types of kites (figure 9(a)) were tested in order to find the one that best suited the objective of the project and the final choice was a conyne kite. The mechanism used for the system to convert wind energy into mechanical energy was also studied by the team.

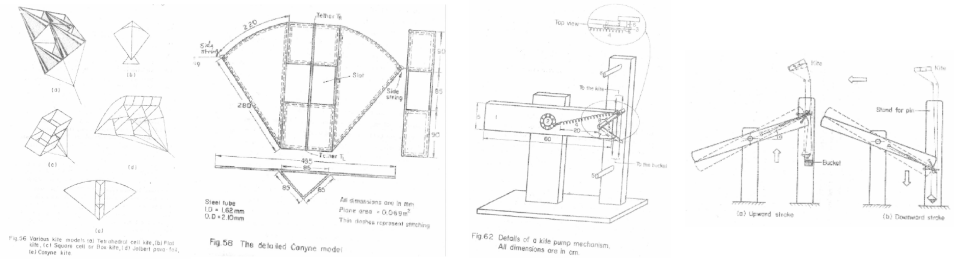

(a) Prototypes (b) Prototype spring

Figure 9: Goela prototype, figures from [15]

A mechanism for converting motion into energy (wind into mechanical) was designed. It consisted on a balanced beam with a support point and a loaded spring. Figure 9(b) the mechanism and its working principle can be seen. Springs were used to change the motion of the kite, from ascent to descent and vice-versa, by switching the angle of attack.

This was the beginning of the energy generation by kites. In 1983 the control system of the kite was a mechanism made by a spring and 20-30 years later, it can be controlled automatically by computers.

1.1.5.2 KiteGen

KiteGen project has been introduced before with the turntable kite model, the carousel configuration. This project not only develops this configuration, but it also includes simple kite systems. KiteGen project born at Politecnico di Torino to design and build a new class of wind energy generators in collaboration with Sequoia Automation, Modelway and Centro Studi Industriali. Its founder was the Doctor Massimo Ippolito.

KiteGen project has developed a small-scale prototype, shown at figure 10(a). Kite is controlled with the pulling force at each line. This lines are rolled to two drums of the ground station and linked to one each electric drives.

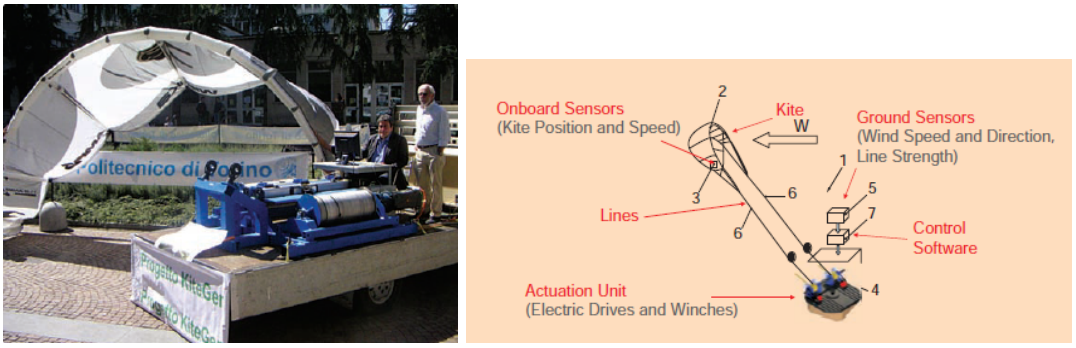

(a) Prototype (b) KSU

Figure 10: KiteGen prototype, figures from [9]

This configuration is under the control of a kite steering unit (KSU), shown at figure 10(b). The maximum length of wires is 300 m and when it is reached, the systems activate motors to reel-back the wire and do the cycle again.

1.1.5.3 Delft University

This university is the more visible investigation group in the energy production environment by AWES. Delft University also collaborate in the group KitePower. This group has some investigation lines of kite design, aerodynamic, control, simulation, earth station and on-board measurement. Its current prototype, which can be transportable, is able to generate 20kW.

Delft University works also in the academic environment, which means that they are also able to investigate in this way. Actually they are developing and improving the control of the kite, they are making studies about the viability and improving hardware and systems.

They also work in the automation of the control by lines and carry them from a hanging box of the kite allows to have the control only by one line, simplifying it. This means that the model is based on a principal line with a control box in its end from where two short flanges arise to attach the kite. To construct the model in that way let have control in the box which has the necessary equipments to operate with the flanges.

The work of Delft is extent in the environment of simulation and software. They also work in aerodynamic studies and finite element methods in structure deformation in aerodynamics. Respect to dynamic simulators, Delft University shows that a visual simulator at real time is a complex work subjected to a lot of exhaustive revisions. This tool is very important in the building of a new prototype.

Apart of the structural simulator for the study of the deformation of flexible kites (two examples in figure 11), Delft team owns two simulators. One of them is a static simulator for the calculation and evaluation of the efforts; the other one is a dynamic one for the study of the motion of the kite.

Figure 11: Delft kites, figure from [16]

1.2 Objectives of the project

In this Bachelor Thesis a model of a kite linked by two wires has been developed. The kite is a rigid solid, flexibility is not considered, and the wires are inextensible and their mass negligible. The difference of present model with the one used by [5] is that this kite is attached at two different points by two wires joined to the ground station in the other end. Wires' initial length is going to play an important role when finding dimensionless variables. They can be used to control the kite with respect to time, but in this Bachelor Thesis, this situation is not considered.

This project is divided in different sections which explain step by step the kite model, the equations of motion and the stability of the kite at equilibrium. Kite model and shape have been explained and analysed. Kite shape coincides with the one used by [5] and it is build up by chord, span and height. Center of mass of kite must be located by using kite parameters and also its mass. Kite can be placed in the space with parameters and position of center of mass. Center of mass is the origin of the body frame, which is reached from earth fixed reference frame after 4 rotations (going through auxiliary frames), the 4 angles corresponding to the state vector and the degrees of freedom (6 dof of a rigid body minus two constraints). Control vector, which is not used in a time dependent way in this Bachelor Thesis, is also calculated being time dependent. Solid kinematics have been developed by calculating angular velocities associated to the different rotations, position vector of the center of mass with respect to the inertial earth frame and also velocity vector, by deriving position vector with respect to time in earth frame.

In next section equations of motion are going to be discuss. Center of mass acceleration was not calculated because the used formulation is the Lagrangian, and it does not use accelerations. This formulation is also characterized because of the elimination of traction forces. Lagrangian function is composed by kinetic and potential energy. Kinetic energy is given by linear and angular velocities; potential energy can be calculated from position vector. From Lagrangian formulation, equations of motion can be calculated.

Finally, for studying the stability of the kite, equilibrium positions must be calculated. They come up after solving equations of motion using Newton's method, assuming some statements. At this equilibrium point the problem must be analysed and Jacobian is obtained. The Jacobian is a matrix to which eigenvalue problem is applied. For finding the stability boundary in terms of wind velocity, real part of eigenvalues is plotted versus different values of wind velocity. The point at which real part of all eigenvalues become negative, is the one that sign the stability limit. An analysis in the stable region is also performed, solving the eigenvalue problem and finding the different modes which explain the behaviour of the kite in that equilibrium point at some stable velocity. For finishing the complete study of stability, the response of the kite after a perturbation from the equilibrium point is analysed in stable and unstable region, finding that in stable region, motion tends to be convergence and in unstable region, motion will be divergence.

2 Preliminary background

2.1 Introduction

In this section, kite model has been discussed. Kite geometry is introduced for the calculation of the center of mass of kite, the point that must be located in space in order to locate the kite. By knowing the position of the center of mass (G) and kite dimensions the position of the rest of the kite points can be placed because there are no deformations along time, kite is a rigid solid. The principal characteristic of a rigid solid is that all points remain in constant position during time, there is not flexibility and it can be placed in space by giving 6 coordinates. Inertia tensor must be also calculated for performing the kite motion analysis. This inertia tensor is diagonal which is possible because of the placement of the body frame, coinciding with the principal axes of inertia.

Different coordinate systems must be used for locating the kite in the space. Between the inertial Earth reference frame and body frame, auxiliary frames are defined. This model is attached to two wires which act like constraints; and this constraints eliminate degrees of freedom (dof) of the rigid solid, so system has 4 dof. These freedoms corresponds to the rotations that must be done for placing G in the space by looking from the inertial Earth frame. These rotations give up angular velocities of the system.

The angles of the four rotation build the state vector which, together with the control vector, a vector with two variables that depend on time, allows to locate the kite position. Vector position must be derived in time for obtaining the velocity of the center of mass of the kite. This process contains non-inertial frames, and velocity must be calculated respect to an inertial frame, so Coriolis Theorem is applied.

All used values are dimensionless. Lengths are dimensionless dividing by the initial length of tethers, L_0. Formulation efficiency and compactness are improved by denoting with a dot the derivative of a variable with respect to the dimensionless time:

$$\tau \equiv \sqrt{\frac{g}{L_0}}t$$

For instance, we will write $\dot{a}$ instead of $\mathrm{d}a/\mathrm{d}\tau$. Term $\sqrt{\frac{L_0}{g}}$, where g is the gravity acceleration, will be characteristic time t^* used for dimensionless time quantities. For brevity, the sine and cosine of an angle α will be written as $s\alpha$ and $c\alpha$. In general, lower case letters will be used to denote dimensionless quantities.

2.2 Kite geometry

Kite geometry play an important role in kite motion. Kite can be modelled by knowing its shape and its parameters. Its shape is an elliptical one and its parameters are span, height and chord. The value of this parameters does not change because kite is a rigid solid, its shape is constantly the same. Kite has two planes of symmetry, one of them perpendicular to chord and the other one perpendicular to span.

It is important to stand out that, as introduced before, lower case letters denote dimensionless quantities. Chord (c), span (b) and height (h) are dimensionless parameters; recall that for obtaining dimensionless length parameters, they must be divided by L_0. These parameters can be seen graphically at figure 12(a). Height and span also define the cross section of the kite. This cross section is a semi-ellipse which can be seen in figure 12(b). This semi-ellipse can be given by equation 1 but firstly drawing a new reference frame in 2D (ξ, ψ), shown also in figure 12(b).

$$\left(\frac{2\xi}{b}\right)^2 + \left(\frac{\psi}{h}\right)^2 = 1 \tag{1}$$

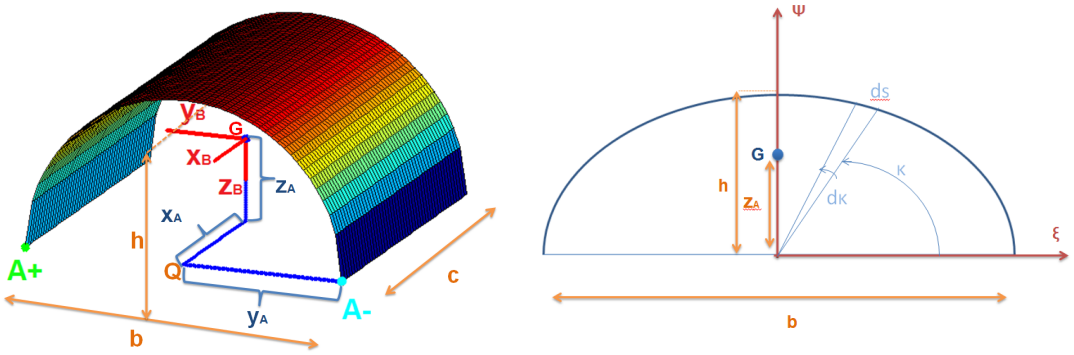

(a) Kite geometry

(b) Elliptical cross section

Figure 12: Kite model

The introduced frame is, as kite parameters, dimensionless and it is very useful for computing the value of z_A, the height of the center of mass. Center of mass position of the kite must be determined. This point is the one used for placing kite in space and its position with respect to kite geometry is important to place the whole kite.

2.2.1 Center of mass

Center of mass position must be calculated in kite by three coordinates. Two of them can be easily known because of the symmetry of the kite about span and chord-wise directions; the last coordinate, center of mass height, cannot be calculated easily because of the absence of symmetry with respect to the perpendicular plane of this direction. The value of x_A is the dimensionless semi-chord (c/2), y_A is the dimensionless semi-span (b/2), see figure 12(a).

For calculating the value of z_A the elliptical cross section must be analysed. For the calculation, property of constant mass distribution must be considered. The position is obtained by integrating the unknown coordinate of the point with respect to the differential of mass which can be substituted by the superficial density by dimensionless chord, c, by the differential length of the semi-ellipse, ds. The expression must be divided by the whole mass of the kite M with the purpose of dimensionless the parameter:

$$z_A = \frac{1}{M} \int \psi dm = \frac{\sigma c}{M} \int \psi ds \tag{2}$$

Where the superficial density is:

$$\sigma = \frac{M}{S} = \frac{M}{c \cdot \lambda} \tag{3}$$

In equation 3 the value of λ is an unknown. This parameter is the length of the semi-ellipse, so for compute the value of λ ds must be integrated between 0 and π, the angle range that the semi-ellipse covers. For computing ds, new frame coordinates must be written as a function of dimensionless height (h), dimensionless semi-span (b/2) and angle κ, the one with range 0 to π which follows the length of the semi-ellipse, it can be seen in figure 12(b). They must be differentiated because ds is calculated from the differential of each coordinate:

$$\begin{aligned} \xi = \frac{b}{2} c\kappa \rightarrow d\xi = -\frac{b}{2} s\kappa \; d\kappa \\ \psi = hs\kappa \rightarrow d\psi = h \; c\kappa \; d\kappa \end{aligned} \tag{4}$$

As said before, ds depend on $d\xi$ and $d\psi$. It is calculated like a modulus of the differential position:

$$ds = \sqrt{d\xi^2 + d\psi^2} = \frac{b}{2}\sqrt{sin^2(\kappa) + \frac{2h}{b}cos^2\kappa}\ d\kappa \equiv \frac{b}{2}f(\kappa)d\kappa \tag{5}$$

It is used to compute the whole length of the semi-ellipse λ by integrating along the range of κ:

$$\lambda = \int_0^\pi ds = \frac{b}{2}\int_0^\pi f(\kappa)d\kappa \approx \frac{\pi}{2}\left[3\left(\frac{b}{2}+h\right) - \sqrt{\left(3\frac{b}{2}+h\right)\left(\frac{b}{2}+3h\right)}\right] \tag{6}$$

And finally, this parameter is introduced in equation 2 together with all needed parameters to obtain the value of z_A:

$$z_A = \frac{\sigma\ c\ h\ b}{2M}\int_0^\pi s\kappa f(\kappa)d\kappa \tag{7}$$

2.2.2 Moments of inertia

There are three principal directions or axes about which kite can rotate; these are the principal axes of inertia. The tensor of inertia of the body must be computed with respect to center of mass. For convenience, the tensor matrix is chosen to be diagonal. For that purpose, the axis of the body frame must coincide with the principal axes of inertia.

Dimension matrix is $\boldsymbol{I_G}$ which can be written as $\boldsymbol{I_G} = ML_0^2\boldsymbol{i_G}$ where $\boldsymbol{i_G}$ is the dimensionless matrix, the one used, as all parameters in this Bachelor Thesis. The form of this dimensionless matrix reads:

$$\boldsymbol{i_G} = \begin{pmatrix} I_{xx} & 0 & 0 \\ 0 & I_{yy} & 0 \\ 0 & 0 & I_{zz} \end{pmatrix} \tag{8}$$

Where I_{xx} is the moment of inertia with respect to x-axis of body frame, I_{yy} is computed with respect to y-axis of body frame and I_{zz} is calculated with respect to vertical z-axis. For calculating the moment of inertia with respect an axis, the summation of the square of both coordinates perpendicular to the axis is made with respect to the differential of mass of the kite. For keeping on with the dimensionless form, coordinates must be substituted by dimensionless parameters defined before; and the complete expression must be divided by the whole mass of the kite. The three equations for calculating this three terms read:

$$\begin{aligned} I_{xx} &= \frac{1}{M}\int\int_A (y_B^2 + z_B^2)dm = \sigma c\frac{b^3}{8}\int_0^\pi \left(cos^2\kappa + \frac{2h}{b}sin^2\kappa\right)f(\kappa)d\kappa \\ I_{yy} &= \frac{1}{M}\int\int_A (x_B^2 + z_B^2)dm = \sigma c\frac{b}{2}\left[\frac{c^2}{12}\int_0^\pi f(\kappa)d\kappa + \int_0^\pi (h_G - hsin\kappa)^2 f(\kappa)d\kappa\right] \\ I_{zz} &= \frac{1}{M}\int\int_A (x_B^2 + y_B^2)dm = \sigma c\frac{b}{8}\left[\frac{c^2}{3}\int_0^\pi f(\kappa)d\kappa + b^2\int_0^\pi cos^2\kappa f(\kappa)d\kappa\right] \end{aligned} \tag{9}$$

2.2.3 Attached points and wires

The principal characteristic of this Bachelor Thesis kite, the concept of two attached wires, suppose two attached points in the kite. These wires are joined in the other end to ground station. Attached points at kite can be observed in figure 12(a) as A_+ and A_-.

All points in kite are express in coordinates of the frame attached to the body. This frame has its origin at the center of mass (G) so points A_+ and A_- must be expressed in body coordinates. The value of each coordinate corresponds to the previously calculated x_A, y_A and z_A, so vector that denotes the position of attached points reads:

$$\overline{GA_\pm} = x_A \boldsymbol{i_B} \pm y_A \boldsymbol{j_B} + z_A \boldsymbol{k_B} \tag{10}$$

In the other hand, the other end of wires, as said before, is attached to Earth. This point at which wires are joined marks the origin of the Earth reference frame. Both reference systems mentioned in this section must be completely explained together with the relation between them; next section 2.3 explain all used reference frames and the relation between them.

2.3 Coordinate systems

A frame of reference is, according to [17], a set of coordinates used to measure things that matter in Newtonian problems. One special type is the inertial frame, where Newton's law of inertia holds, also as [17] establishes. In the other hand, a non-inertial frame is a frame that is rotating. In this system, Earth frame can be identify as an inertial frame, and body frame together with all auxiliary frames used can be considered non-inertial frames.

Earth frame S_E has its origin in ground station at which wires are joined, calling this point O_E; x-axis (x_E) is parallel to wind velocity but opposite direction, z-axis (z_E) points downwards perpendicularly to Earth assuming that it is flat, finally, y-axis (y_E) fulfils right hand rule to complete this reference frame which can be observed in figure 13(a).

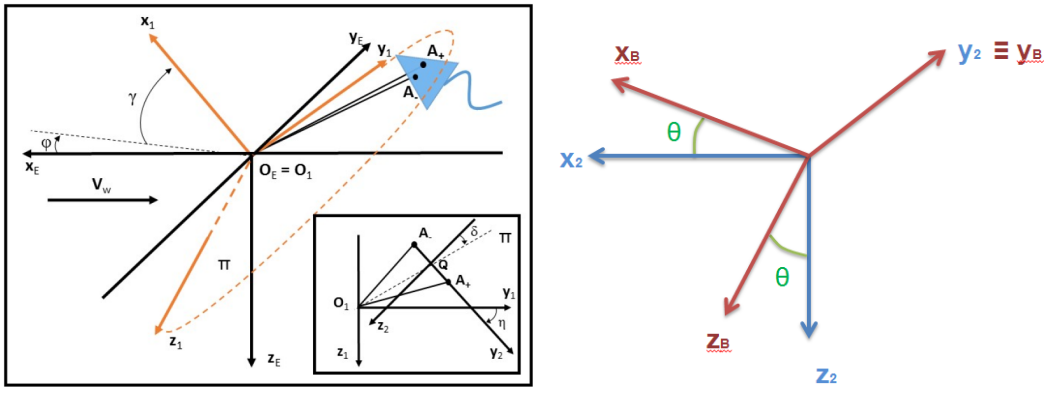

(a) First three rotations

(b) Rotation from S_2 to S_B

Figure 13: Rotations

First auxiliary frame S_1 has same origin as S_E and it comes up after two rotations of the original S_E frame. First rotation is performed about z_E-axis by an angle φ. Second rotation of angle γ is made about y_1-axis, which is the resultant y-axis after the first rotation. Both rotations are expressed together with the reference frame S_1 in of figure 13(a). These rotations generate a matrix to express them simultaneously with an angular velocity associated to the rotation:

$$R_{1E} = \begin{pmatrix} c\gamma c\varphi & c\gamma s\varphi & -s\gamma \\ -s\varphi & c\varphi & 0 \\ s\gamma c\varphi & s\gamma s\varphi & c\gamma \end{pmatrix}$$
$$\boldsymbol{\Omega_{1E}} = \sqrt{g/L_0}(\dot{\varphi}\boldsymbol{k_E} + \dot{\gamma}\boldsymbol{j_1}) \equiv \sqrt{g/L_0}\ \boldsymbol{\omega_{1E}} \tag{11}$$

This new frame defines a plane at $x_1 = 0$ inside where a virtual line formed by points A_+ and A_- is content. This plane called π is expressed in two different ways in figure 13(a); it is expressed in 3D in the principal figure and also in 2D in auxiliary figure attached to that. This auxiliary figure shows also the next reference frame S_2. This frame change its origin from O_E (or O_1) to Q, the middle point between A_+ and A_-; x-axis (x_2) coincides with x_1 which means that rotation is made positively around this axis. The rotation angle is η expressed between y_1 and y_2 in the mentioned figure and lead into a rotation matrix and angular velocity that read:

$$R_{21} = \begin{pmatrix} 1 & 0 & 0 \\ 0 & c\eta & s\eta \\ 0 & -s\eta & c\eta \end{pmatrix}$$
$$\boldsymbol{\Omega_{21}} = \sqrt{g/L_0}\ \dot{\eta}\boldsymbol{k_1} \equiv \sqrt{g/L_0}\ \boldsymbol{\omega_{21}} \tag{12}$$

Finally, for reaching body reference frame, after departing from Earth frame, a last rotation must be performed. This rotation is done about y_2-axis by an angle θ, which can be seen in figure 13(b). This rotation, as the previous ones, create a rotation matrix and also an angular velocity:

$$R_{B2} = \begin{pmatrix} c\theta & 0 & -s\theta \\ 0 & 1 & 0 \\ s\theta & 0 & c\theta \end{pmatrix}$$
$$\boldsymbol{\Omega_{B2}} = \sqrt{g/L_0}\ \dot{\theta}\boldsymbol{j_2} \equiv \sqrt{g/L_0}\ \boldsymbol{\omega_{B2}} \tag{13}$$

Body reference frame is expressed for clarify with same origin as S_2 frame in figure 13(b), but, as introduced in section 2.2, body frame has its origin in the center of mass of kite which obviously does not coincide with Q, as can be seen in figure 12(a). Point Q position can be expressed in body coordinates as $\overline{GQ} = L_0(x_A\boldsymbol{i_B} + z_A\boldsymbol{k_B})$. For completely define body frame, axes positions, as previously introduced, coincide with principal axes of inertia of kite; this means that x_B-axis is chord-wise direction going from G to the front part of the kite (cross section at which attached points are); z_B-axis goes downwards following the direction of kite's height; and y_B-axis fulfils right hand rule. This axes can be seen in figure 12(a).

2.4 Kinematics

Kite in this Bachelor Thesis is a rigid solid, no deformations nor flexibility are considered. The contribution of flexibility in kite has been studied by [16]. A rigid solid can be placed in space by giving 6 coordinates, which means that it has 6 degrees of freedom (dof); but in present model there are two constraints, both wires act as restriction for kite eliminating 2 dof to the system.

Resulting four degrees of freedom coincide with the four rotations made to system, the four angles explained in section 2.3. This angles build up the state vector:

$$\boldsymbol{x_S} = [\varphi\ \gamma\ \eta\ \theta]^T \tag{14}$$

This state vector allows to place the kite in space. Its variables are divided in longitudinal and lateral terms. Longitudinal ones are γ and θ; and lateral variables are φ and η. The summation of longitudinal variables results into the angle of attack of the kite. This state vector has played an important role while expressing position and velocity vectors which are also written as a function of the control vector.

Control vector contains only two variables which are responsible of the control of the kite made from ground station and which depends on time. This variables that compose the vector appear naturally with kite motion and they can be seen in sketch attached to figure 13(a). They are the dimensionless distance between O_1 and Q (l) and angle δ:

$$\boldsymbol{x_c}(t) = [l(t)\ \delta(t)]^T \tag{15}$$

First parameter, l(t), corresponds to the median of the triangle formed by both wires and virtual line formed by points A_+ and A_-. For that to be dimensionless, quantities with same property must be used to calculate l(t) expression. It depends on the length of both wires ($l_{A_+}(t)$ and $l_{A_-}(t)$ in dimensionless form), which vary with time when control is activated, and the fixed parameter y_A:

$$l(t) = \sqrt{\frac{1}{2}(l_{A_+}(t)^2 + \ l_{A_-}(t)^2 - 2 \cdot y_A^2)} \tag{16}$$

Second parameter, angle $\delta(t)$, depends also on time as it depends on same parameters than l(t) and also on l(t) itself:

$$\delta(t) = arsin\left[\frac{l_{A_+}(t)^2 - l_{A_-}(t)^2}{4l(t)\ y_A}\right] \tag{17}$$

Angular velocities play an important role in terms of kinematics. They appear when a rotation takes place and they are applied to relate reference systems. In section 2.3, equations 11, 12 and 13 express the three angular velocities that appear during rotations. All of them must be summed to get the angular velocity that relates body and Earth frames. The expression reads:

$$\boldsymbol{\Omega_{BE}} = \boldsymbol{\Omega_{B2}}+\boldsymbol{\Omega_{21}}+\boldsymbol{\Omega_{1E}} = \sqrt{g/L_0}(\dot{\varphi}\boldsymbol{k_E}+\dot{\gamma}\boldsymbol{j_1}+\dot{\eta}\boldsymbol{i_2}+\dot{\theta}\boldsymbol{j_B}) = P\boldsymbol{i_B}+Q\boldsymbol{j_B}+R\boldsymbol{k_B} = \sqrt{g/L_0}\,\boldsymbol{\omega} \tag{18}$$

$$\boldsymbol{\omega} \equiv \boldsymbol{\Phi}\ \dot{\boldsymbol{x}}_{\boldsymbol{s}} \tag{19}$$

Where:

$$\boldsymbol{\Phi} = \begin{pmatrix} -c\gamma c\eta s\theta - s\gamma c\theta & s\eta s\theta & c\theta & 0 \\ c\gamma s\eta & c\eta & 0 & 1 \\ c\gamma c\eta c\theta - s\gamma s\theta & -s\eta c\theta & s\theta & 0 \end{pmatrix} \tag{20}$$

Position vector of kite is computed as the position of the center of mass of it with respect to Earth frame ($\overline{O_EG}$). This vector, for calculate it easily, can be split in two, $\overline{O_EQ}$ and $\overline{QG}$, which are respectively the position of point Q with respect to Earth and the inverse of the position of Q with respect to body frame. Position vector reads:

$$\boldsymbol{R_G} = \overline{O_EG} = \overline{O_EQ} + \overline{QG} \equiv L_0\boldsymbol{r_G} \tag{21}$$

Where vector $\overline{O_E Q}$ can be seen in figure 13(a) and vector $\overline{QG}$ was introduced in section 2.3. They read:

$$\begin{aligned} \overline{O_E O_2} &= L_0\ l(sin(\eta+\delta)\boldsymbol{j_1} - cos(\eta+\delta)\boldsymbol{k_1}) \\ \overline{O_2 G} &= -L_0(x_A \boldsymbol{i_B} + z_A \boldsymbol{k_B}) \end{aligned} \tag{22}$$

It is interesting to keep position vector with the same separated form in order to find in an easier way the velocity vector. Velocity vector must be calculated regarding an inertial frame by deriving position vector. As both parts of position vector are not expressed in Earth frame coordinates, Coriolis theorem must be applied:

$$\boldsymbol{V}_G = \left.\frac{d\boldsymbol{R}_G}{dt}\right|_{SE} = \left.\frac{d\overline{O_E O_2}}{dt}\right|_{S1} + \boldsymbol{\Omega}_{1E} \wedge \overline{O_E O_2} + \left.\frac{d\overline{O_2 G}}{dt}\right|_{SB} + \boldsymbol{\Omega}_{BE} \wedge \overline{O_2 G} \equiv \sqrt{gL_0}\ \boldsymbol{v_G} \tag{23}$$

Term $\sqrt{gL_0}$ is known as characteristic velocity V^* and it is used to dimensionless velocities. Dimensionless velocity $\boldsymbol{v_G}$ must be written in the form of a matrix by the derivative of state vector plus another matrix by derivative of control vector.

$$\boldsymbol{v}_G \equiv \boldsymbol{\Upsilon_S} \cdot \dot{\boldsymbol{x}}_{\boldsymbol{S}} + \boldsymbol{\Upsilon_C} \cdot \dot{\boldsymbol{x}}_{\boldsymbol{C}} \tag{24}$$

Where matrices are:

$$\boldsymbol{\Upsilon_S}(\boldsymbol{x_s}, \boldsymbol{x_c}) = \begin{pmatrix} l(s\delta s\gamma s\theta - c\gamma s(\eta+\delta)c\theta) - z_A c\gamma s\eta & -lc(\eta+\delta)c\theta - z_A c\eta & -ls\delta s\theta & z_A \\ s\gamma(x_A s\theta - z_A c\theta - lc\delta) - c\gamma c\eta(x_A c\theta + z_A s\theta) & s\eta(x_A c\theta + z_A s\theta) & lc\delta - x_A s\theta + z_A c\theta & 0 \\ -l(s\delta s\gamma c\theta + c\gamma s(\eta+delta)s\theta) + x_A c\gamma s\eta & -lc(\eta+\delta)s\theta + x_A c\eta & ls\delta c\theta & x_A \end{pmatrix} \tag{25}$$

$$\boldsymbol{\Upsilon_C}(\boldsymbol{x_s}, \boldsymbol{x_c}) = \begin{pmatrix} c\delta s\theta & -ls\delta s\theta \\ s\delta & lc\delta \\ -c\delta s\theta & ls\delta c\theta \end{pmatrix} \tag{26}$$

3 Equations of motion

3.1 Introduction

This section presents the equations of motion of two-line kite. This kite model was constructed by [18] and now on the more important steps for finding equations of motion which are used in section 4 for investigating kite dynamics. Two possibilities in terms of choosing formulation were debated, classical formulation and Lagrange formulation. This last one is chosen for the purpose of writing the equations because it eliminates the contribution of wires in equations. This section feeds on previous one for computing both aerodynamic model and dynamic equations. For calculating aerodynamic forces and moments, aerodynamic velocity must be computed by adding the contribution of wind velocity.

Aerodynamic coefficients have played an important role in forces and moments calculations as well as dimensionless body frame components of total angular velocity (p, q and r) which can be obtained from section before and dimensionless it by using kite parameters (b and c) and reference velocity V_T.

Angle of attack (α) and sideslip angle (β) are both utilized for multiplying their derivatives of aerodynamic coefficients; these angles depend only on aerodynamic velocity. Aerodynamic moment, or torque, must be multiplied by length as definition of torque requires (force by distance), so kite parameters chord and span should be used for obtaining the result of torque.

With these force and moment together with vector position, and linear and angular velocities Lagrangian function can be build up. This function concerns kinetic and potential energies written as a function of state and control vectors for easily defining the four equilibrium equations needed.

3.2 Aerodynamic model

There are forces and moments acting on kite. Weight, tethers tension and aerodynamic forces and moments are which act on kite. In this section, aerodynamic contributions in kite have been studied. They are an essential part of model formulation, they contribute to build generalized forces in Lagrange formulation. Their dimension form is:

$$\boldsymbol{F_A} = \frac{1}{2}\rho S V_A^2 \boldsymbol{F'_A} \tag{27}$$

$$\boldsymbol{M_A} = \frac{1}{2} L_0 \rho S V_A^2 \boldsymbol{M'_A} \tag{28}$$

Where S is the surface of kite, ρ is the air density, V_A is the aerodynamic velocity, $\boldsymbol{F'_A}$ is the dimensionless aerodynamic force and $\boldsymbol{M'_A}$ is the dimensionless aerodynamic moment. Aerodynamic velocity comes from the composition between velocity of center of mass and wind velocity. Wind velocity is aligned with x_E-axis but opposite direction. Its expression reads:

$$\boldsymbol{V_w} = -\sqrt{gL_0}\ v_w \boldsymbol{i_E} \equiv \sqrt{gL_0}\ \boldsymbol{v_w} \tag{29}$$

Where $\boldsymbol{v_w}$ is the dimensionless wind velocity. This term, together with dimensionless center of mass velocity $\boldsymbol{v_G}$, forms the dimensionless aerodynamic velocity:

$$\boldsymbol{v_A} = \boldsymbol{v_G} - \boldsymbol{v_w} \tag{30}$$

According to equations 27 and 28, dimensionless aerodynamic forces and moments only depend on dimensionless aerodynamic coefficients (c_{x_0}, c_{z_0} and c_{m_0}), aerodynamic force coefficients (c_{x_α}, c_{y_β} and c_{z_α}), aerodynamic moment coefficient (c_{l_β}, $c_{l_{p'}}$, c_{m_α}, $c_{m_{q'}}$, c_{n_β} and $c_{n_{r'}}$), dimensionless

kite parameters (b and c), dimensionless angular velocities (p, q and r), angle of attack (α) and sideslip angle (β). Angular velocities, introduced in equation 18, must be dimensionless to be used in aerodynamic forces and moments; these components of total angular velocity in body frame can be dimensionless by using kite parameters (b and c) and reference velocity (V_T); calculations can be observed in equation 31.

$$\begin{aligned} p &= \frac{P\ b}{2V_T} \\ q &= \frac{Q\ c}{V_T} \\ r &= \frac{R\ b}{2V_T} \end{aligned} \tag{31}$$

Angle of attack (α) is the angle at which kite faces wind; it is calculated by x and z aerodynamic velocity components, see equation 32. Sideslip angle is the angle from which aerodynamic velocity approaches kite; it is calculated by the contribution of y component of aerodynamic velocity and its modulus, see also equation 32.

$$\begin{aligned} \alpha &= arctan\left(\frac{\boldsymbol{v_A}\cdot\boldsymbol{k_B}}{\boldsymbol{v_A}\cdot\boldsymbol{i_B}}\right) \\ \beta &= \ arcsin\left(\frac{\boldsymbol{v_A}\cdot\boldsymbol{j_B}}{|\boldsymbol{v_A}|}\right) \end{aligned} \tag{32}$$

Dimensionless aerodynamic forces and moments, as said above, depend on the explained parameters and they read:

$$\boldsymbol{F'_A} = (C_{x0} + C_{x\alpha}\alpha)\boldsymbol{i_B} + C_{y\beta}\beta\boldsymbol{j_B} + (C_{z0} + C_{z\alpha}\alpha)\boldsymbol{k_B} \tag{33}$$

$$\boldsymbol{M'_A} = b(C_{l\beta}\beta + C_{lp}p)\boldsymbol{i_B} + c(C_{m0} + C_{m\alpha}\alpha + C_{mq}q)\boldsymbol{j_B} + b(C_{n\beta}\beta + C_{nr}r)\boldsymbol{k_B} \tag{34}$$

For convenience, aerodynamic force is expressed by dimensionless form by mass and gravity; and aerodynamic moment can be computed as a dimensionless form by mass, gravity and initial length of wires. They read:

$$\begin{aligned} \boldsymbol{F_A} &= Mg\boldsymbol{f_A} \\ \boldsymbol{M_A} &= MgL_0\boldsymbol{m_A} \end{aligned} \tag{35}$$

For this new expression, two terms must multiply equations 33 and 34. These terms are the square modulus of aerodynamic velocity (v_A^2) and μ which is a dimensionless parameters that includes air density (ρ), kite surface (S), initial tethers length (L_0) and mass (M), reading the term $\rho SL_0/2M$. Final expression of dimensionless aerodynamic forces and moment are:

$$\boldsymbol{f_A} = \mu v_A^2 \left[(C_{x0} + C_{x\alpha}\alpha)\boldsymbol{i_B} + C_{y\beta}\beta\boldsymbol{j_B} + (C_{z0} + C_{z\alpha}\alpha)\boldsymbol{k_B}\right] \tag{36}$$

$$\boldsymbol{m_A} = \mu v_A^2 \left[b(C_{l\beta}\beta + C_{lp'}p)\boldsymbol{i_B} + c(C_{m0} + C_{m\alpha}\alpha + C_{mq'}q)\boldsymbol{j_B} + b(C_{n\beta}\beta + C_{nr'}r)\boldsymbol{k_B}\right] \tag{37}$$

3.3 Dynamic equations of kite

3.3.1 Lagrangian formulation

For conservative systems, there is an elegant formulation of classical mechanics known as the Lagrangian formulation. The Lagrangian function, $\mathscr{L}$, for a system is defined to be the difference between the kinetic and potential energies expressed as a function of positions and velocities. The Lagrangian is defined as follows:

$$\frac{d}{d\tau}\left(\frac{\partial \mathscr{L}}{\partial \dot{x}_{si}}\right) - \frac{\partial \mathscr{L}}{\partial \dot{x}_{si}} = Q_i \tag{38}$$

So, keeping on with the definition, Lagrangian function reads:

$$\mathscr{L} = e_k - u_p \tag{39}$$

Total kinetic energy of the kite system, which consists on translational and rotational energy, is obtained by substituting in the following equation linear and angular velocities:

$$e_k = \frac{1}{2}|\boldsymbol{v_G}|^2 + \frac{1}{2}\boldsymbol{\omega}^T \cdot \boldsymbol{i_G} \cdot \boldsymbol{\omega} \tag{40}$$

The equation on terms of state and control vectors and its derivatives, by substituting velocities, reads:

$$e_k(\boldsymbol{x_s}, \boldsymbol{x_c}, \dot{\boldsymbol{x}}_{\boldsymbol{s}}, \dot{\boldsymbol{x}}_{\boldsymbol{c}}) = \frac{1}{2}\left(\dot{\boldsymbol{x}}_{\boldsymbol{s}}^T \cdot \boldsymbol{M_{ss}} \cdot \dot{\boldsymbol{x}}_{\boldsymbol{s}} + 2\dot{\boldsymbol{x}}_{\boldsymbol{s}}^T \cdot \boldsymbol{M_{sc}} \cdot \dot{\boldsymbol{x}}_{\boldsymbol{c}} + \dot{\boldsymbol{x}}_{\boldsymbol{c}}^T \cdot \boldsymbol{M_{cc}} \cdot \dot{\boldsymbol{x}}_{\boldsymbol{c}}\right) \tag{41}$$

Where:

$$\begin{aligned} \boldsymbol{M_{ss}} &\equiv \boldsymbol{\Upsilon_S}^T \cdot \boldsymbol{\Upsilon_S} + \boldsymbol{\Phi}^T \cdot \boldsymbol{i_G} \cdot \boldsymbol{\Phi} \\ \boldsymbol{M_{sc}} &\equiv \boldsymbol{\Upsilon_S}^T \cdot \boldsymbol{\Upsilon_C} \\ \boldsymbol{M_{cc}} &\equiv \boldsymbol{\Upsilon_C}^T \cdot \boldsymbol{\Upsilon_C} \end{aligned} \tag{42}$$

Gravitational potential is the potential energy associated with gravitational force, as work is required to elevate objects against Earth's gravity. The definition of gravitational potential reads: $u_p = -\boldsymbol{r_G} \cdot \boldsymbol{k_E}$. By substituting the expression of the position vector in the formula, a final expression for gravitational potential is obtained, reading:

$$u_p(\boldsymbol{x_s}, \boldsymbol{x_c}) = lc\gamma c(\eta + \delta) - x_A\left(s\gamma c\theta + c\gamma s\theta c\eta\right) - z_A\left(s\gamma s\theta - c\gamma c\theta c\eta\right) \tag{43}$$

Right hand side of Lagrangian formula ($\mathbb{Q}_i$) corresponds to generalized forces. This forces depends on aerodynamic force and torque about center of mass, and linear and angular velocities. Getting an expression that reads:

$$Q_i = \boldsymbol{f_A} \cdot \frac{\partial \boldsymbol{v_G}}{\partial \dot{x}_{si}} + \boldsymbol{m_A} \cdot \frac{\partial \boldsymbol{\omega}}{\partial \dot{x}_{si}} \tag{44}$$

Notation of state vector at equations 38 and 44 read $\dot{x}_{si}$ where i is an scalar that goes from 1 to 4, the number of equations that are going to appear in for finding the equilibrium. Term $\frac{\partial \boldsymbol{v_G}}{\partial \dot{x}_{si}}$ is obtained by deriving equation 24 with respect to state vector. By simply deriving with respect to state vector, matrix Υ_S is obtained, but equation 44 need as input a vector; this is why notation with i is applied. The dimension of matrix Υ_S is 3x4, so columns 1 to 4 have been used for each equation. For second term, same procedure has been followed, equation 19 is derived respect to state vector and columns 1 to 4 of matrix Φ and resultant vectors multiply dimensionless torque of equation 37. An example has been performed for understanding this method and notation:

State vector $x_s = [\varphi\ \gamma\ \eta\ \theta]^T$ has terms 1 to 4 that corresponds to angles. The angle chosen for the example is angle θ, so derivatives must be done respect to $\dot{x}_{S4}$ or $\dot{x}_{S\theta}$. Derivative of matrix Υ_S respect to $\dot{x}_{S4}$ is the fourth column of the matrix, expressed in equation 25 which is vector $[z_A\ 0\ x_A]^T$. This vector multiplied by vector $\boldsymbol{f_A}$ reads:

$$z_A \mu v_A^2 (C_{x0} + C_{x\alpha}\alpha) + x_A \mu v_A^2 (C_{z0} + C_{z\alpha}\alpha)$$

Second term is the result of multiplying fourth column of matrix Φ of equation 20 which is vector $[0\ 1\ 0]^T$ by vector $\boldsymbol{m_A}$ of equation 37 with result:

$$\mu v_A^2 c (C_{m0} + C_{m\alpha}\alpha + C_{mq'} q)$$

Obtaining by summation of both terms the final expression for the fourth term of generalized forces.

3.3.2 Lagrange equations of motion

Lagrangian equations of motion can be finally defined by using all the previous data of equations 38, 41, 42, 43 and 44, and combining them. The result is a second order differential equation that involves M matrices, state and control vectors, potential energy and all terms that were introduced in the explanation of generalized forces that reads:

$$\begin{aligned} M_{ss_{ij}} \ddot{x}_{sj} + \left[\frac{\partial M_{ss_{ij}}}{\partial x_{sk}} \dot{x}_{sk} + \frac{\partial M_{ss_{ij}}}{\partial x_{ck}} \dot{x}_{ck} \right] \dot{x}_{sj} + M_{sc_{ij}} \ddot{x}_{cj} + \left[\frac{\partial M_{sc_{ij}}}{\partial x_{sk}} \dot{x}_{sk} + \frac{\partial M_{sc_{ij}}}{\partial x_{ck}} \dot{x}_{ck} \right] \dot{x}_{cj} \\ -\frac{1}{2} \left(\frac{\partial M_{ss_{jk}}}{\partial x_{si}} \dot{x}_{sj} \dot{x}_{sk} + 2 \frac{\partial M_{sc_{jk}}}{\partial x_{si}} \dot{x}_{sj} \dot{x}_{ck} \right) + \frac{\partial u_p}{\partial x_{si}} = f_{Ak} \Upsilon_{S_{ki}} + m_{Ak} \Phi_{ki} \end{aligned} \tag{45}$$

Note that term $\partial M_{cc_{jk}} / \partial x_{si}$ does not appear in the equation, and it is because as seen before, M_{cc} does not depend on state vector. This differential equation is expanded to obtain the four equilibrium equations solved in next section thanks to the use of the software *Matlab*.

For convenience, an extended state vector $\boldsymbol{u}$ is introduced. This vector is formed by state vector and its first derivative, equation 46; and written in a system of first order ordinary differential equations as equation 47 shows. The purpose of doubling the size of the vector is to transform the set of 4 second order equations that comes from equation 45 to 8 equations of first order.

$$\boldsymbol{u} = [\boldsymbol{x}_S\ \dot{\boldsymbol{x}}_S]^T \tag{46}$$

$$\frac{d\boldsymbol{u}}{d\tau} = \boldsymbol{f}(\boldsymbol{u}, \tau; \boldsymbol{p}) \tag{47}$$

4 Kite dynamics

4.1 Introduction

This section studies the dynamics of this kite system. When talking about stability, equilibrium must exist. Equilibrium, according to [19], denotes a steady state of the system, at which all the state variables are constant in time.

Equilibrium positions are calculated by solving the two non-trivial equations from the set of 8 equations obtained in previous section. These equations come out after taking into account some assumptions introduced in this section. The stability of the solution must be studied by perturbing it and solving a linear system that is transformed into an eigenvalue problem by obtaining the Jacobian matrix evaluated at the equilibrium point.

Obtained Jacobian matrix near equilibrium point is disengaged and it differentiates lateral and longitudinal problems. The stability analysis is performed separately to both motions, lateral and longitudinal. In both analysis, modes are obtained and studied.

Finally, a non-linear analysis is performed for evaluate the equilibrium by exciting all modes. The analysis is computed in the stable and unstable regions. For the stable region, the result must fulfil the expectations, to converge in a determined value. In case of unstable region, motion diverges from the equilibrium point and it reaches a periodic orbit. In table 2, dimension values can be founded, but for all calculations, parameters acquire the dimensionless values introduced in table 3.

C	1.5 m	B	5.8 m	H	3.2 m
M	3 kg	X_A	0.75 m	Y_A	2.9 m
Z_A	2.0039 m	S	14.3815 m^2	L_0	200 m
g	9.81 m/s^2	ρ	1.225 kg/m^3	V_T	7 m/s
t^*	4.5152 s	V^*	44.2945 m/s		

Table 2: Parameters values with dimensions

$\boldsymbol{\mu}$	587.2432	$\boldsymbol{I_{xx}}$	0.0115	$\boldsymbol{c_{l_\beta}}$	-0.49
$\boldsymbol{v_T}$	0.158	$\boldsymbol{I_{yy}}$	0.0054	$\boldsymbol{c_{l_{p'}}}$	-0.15
$\boldsymbol{c}$	0.0075	$\boldsymbol{I_{zz}}$	0.0106	$\boldsymbol{c_{m_0}}$	0.1332
$\boldsymbol{b}$	0.029	$\boldsymbol{c_{x_0}}$	-0.065	$\boldsymbol{c_{m_\alpha}}$	-0.7633
$\boldsymbol{h}$	0.016	$\boldsymbol{c_{x_\alpha}}$	0.176	$\boldsymbol{c_{m_{q'}}}$	-0.165
$\boldsymbol{x_A}$	0.0037	$\boldsymbol{c_{y_\beta}}$	-1.57	$\boldsymbol{c_{n_\beta}}$	-0.027
$\boldsymbol{y_A}$	0.0145	$\boldsymbol{c_{z_0}}$	0.116	$\boldsymbol{c_{n_{r'}}}$	-0.002
$\boldsymbol{z_A}$	0.01	$\boldsymbol{c_{z_\alpha}}$	-2.97		

Table 3: Dimensionless parameters values

4.2 Kite equilibrium states

4.2.1 Introduction

Equilibrium positions are calculated in this section by satisfying that $\boldsymbol{f}$ is equal to zero and some characteristics:

- The angular velocity Ω_{BE} is zero, so p, q and r are zero
- Control is not applied, parameters do not depend on time. Following this assumption, δ is equal to zero and the dimensionless length of tethers is assumed equal to 1
- Lateral angles, φ and η, are zero, as the equilibrium is symmetric
- As position vector do not depend on time, velocity of the center of mass is zero. According to this assumption, the module of the aerodynamic velocity is the same as the module of the wind velocity
- Only two angles must be found as solutions, γ and θ, so only two equations are going to be used

As equilibrium does not depend on time, $\boldsymbol{f}$ must be equal to 0 in equation 47. The set of 8 equations can be reduced to 2 equations, when applying conditions, which must be solved to find equilibrium positions. Equilibrium vector $\boldsymbol{u^*}$ reads $[0\ \gamma^*\ 0\ \theta^*\ 0\ 0\ 0\ 0]^T$ and non-trivial equations to solve in order to reach solutions for equilibrium of γ^* and θ^* are:

$$s\gamma - \mu v_w^2(c\theta(C_{x_0} + C_{x_\alpha}(\gamma+\theta)) + s\theta(C_{z_0} + C_{z_\alpha}(\gamma+\theta))) = 0 \tag{48}$$

$$x_A c(\gamma+\theta)+z_A s(\gamma+\theta)+\mu v_w^2(c(C_{m_0}+C_{m_\alpha}(\gamma+\theta))-z_A(C_{x_0}+C_{x_\alpha}(\gamma+\theta))+x_A(C_{z_0}+C_{z_\alpha}(\gamma+\theta))) = 0 \tag{49}$$

This equations are solved by using Newton's method. It consists on choosing a point of the graph and draw the tangent line of the curve at this point. The tangent line is dragged on until it crosses the x-axis. At the crossing point, a vertical line is made for finding the value of the function at this value of x. Once the point at the curve is again reached the process is repeated until the crossing point at x-axis coincides with the function, this point will be the root. This method is faster than Bisection method.

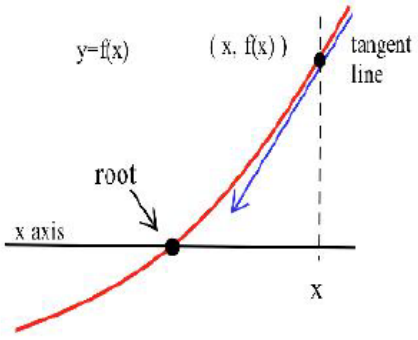

Figure 14: Newton's Method, figure from [20]

For stability study of solutions reached, equilibrium point must be perturbed, vector acquires form $\boldsymbol{u}(\tau) = \boldsymbol{u^*} + \boldsymbol{u_1}(\tau)$, where $\boldsymbol{u_1}(\tau)$ is the small perturbation applied. The behaviour of the kite motion along time is observed for assess if equilibrium point is stable or not. Linear system shown in equation 50 evaluates the problem by Jacobian matrix of $\boldsymbol{f}$ at equilibrium.

$$\frac{d\boldsymbol{u_1}}{d\tau} = \boldsymbol{J}(\boldsymbol{u^*}) \cdot \boldsymbol{u_1} \tag{50}$$

Where $\boldsymbol{J}(\boldsymbol{u^*})$ is the Jacobian matrix evaluated at equilibrium state. It is calculated following the structure expressed in equation 51. Thanks to that matrix, the behaviour of kite can be analysed as an eigenvalue problem.

$$\boldsymbol{J} = \begin{pmatrix} \frac{\partial f_1}{\partial x_1} & \frac{\partial f_1}{\partial x_2} & \cdots & \frac{\partial f_1}{\partial x_n} \\ \frac{\partial f_2}{\partial x_1} & \frac{\partial f_2}{\partial x_2} & \cdots & \frac{\partial f_2}{\partial x_n} \\ \vdots & \vdots & \ddots & \vdots \\ \frac{\partial f_m}{\partial x_1} & \frac{\partial f_m}{\partial x_2} & \cdots & \frac{\partial f_m}{\partial x_n} \end{pmatrix} \tag{51}$$

Jacobian matrix is disengaged in lateral and longitudinal Jacobian matrices of dimension 4x4 as equation 52 shows.

$$\boldsymbol{J} = \begin{bmatrix} \boldsymbol{J_{Lat}} & 0 \\ 0 & \boldsymbol{J_{Lon}} \end{bmatrix} \tag{52}$$

Problem must be examine separately; eigenvalues and vectors of both longitudinal and lateral are calculated. Eigenvalues give the information about stability, if the real part of the eigenvalue is negative, kite is in the stable region. In the other hand, eigenvectors allow to know the information about how is the motion of kite around the equilibrium. Following the stability condition, the angle of attack ($\alpha = \gamma + \theta$) is plotted versus wind velocity for finding the value of wind at which kite enters in the stable region. According to figure 15, the stability boundary is located at dimensionless wind velocity equal to 0.17 where a Hopf bifurcation appears. This kind of bifurcation refers to a local birth or death of a self-excited oscillation.

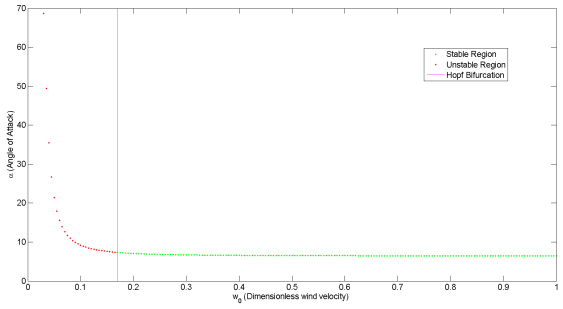

Figure 15: Kite angle of attack versus dimensionless wind velocity

In a differential equation a Hopf bifurcation typically occurs when a complex conjugate pair of eigenvalues of the linearised flow at a fixed point becomes purely imaginary. The form of the Hopf bifurcation is:

$$\frac{dz}{dt} = z((\lambda + i) + b|z|^2) \tag{53}$$

Where z, b are both complex and λ is a parameter. For understanding the Hopf bifurcation in an easier way, a theorem can be exposed: let $\boldsymbol{J}$ be the Jacobian of a continuous parametric dynamical system evaluated at a steady point $\boldsymbol{u^*}$ of it. Supposing that all eigenvalues of $\boldsymbol{J}$ have negative real parts except one conjugate non-zero purely imaginary pair $\pm\beta i$. Following the [21] definition,

a Hopf bifurcation arises when two eigenvalues cross imaginary axis due to a variation of system parameters.

4.2.2 Longitudinal stability analysis

According to [22] complex scalar λ is called an eigenvalue of the square matrix $\boldsymbol{A}$ if there exists a non-zero vector $\boldsymbol{u}$ of C^n such that $\boldsymbol{A} \cdot \boldsymbol{u} = \lambda\, \boldsymbol{u}$. Vector $\boldsymbol{u}$ is called eigenvector of $\boldsymbol{A}$ associated to λ. The set of all the eigenvalues of $\boldsymbol{A}$ is referred to the spectrum of $\boldsymbol{A}$ and is denoted by $\lambda\ (\boldsymbol{A})$.

As introduced before, stability is determined by the real part of eigenvalues. In figure 15, stability limit was previously settled but eigenvalues must be studied for confirm that wind value as the stability boundary. In order to perform that study, real part of eigenvalues must be plotted versus wind velocity; figure 16(a) shows that.

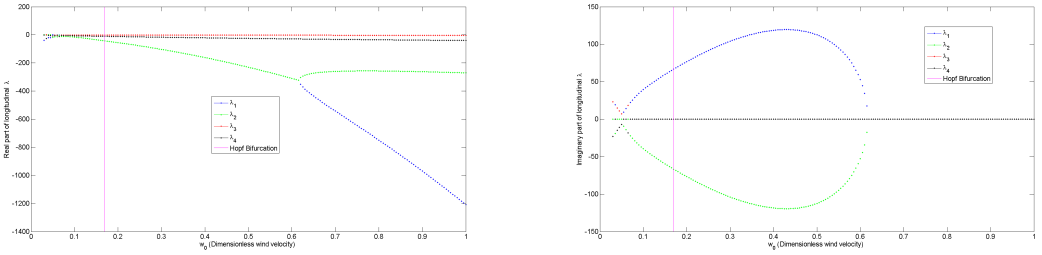

(a) Real part of longitudinal eigenvalues (b) Imaginary part of longitudinal eigenvalues

Figure 16: Longitudinal eigenvalues, both real and imaginary parts separately, versus dimensionlesss wind velocity

What must graph 16(a) present is the value of wind at which curves cross 0 value and become negative. Zoom is needed in order to look for that wind value. Figure 17(a) shows zoomed curves versus the whole interval of wind. This figure allow to observe where the crossing point is, but a more zoomed figure is needed to exactly know what is the wind value researched. Figure 17(b) let see that the value of dimensionless wind velocity at which all eigenvalues have negative real part is 0.04.

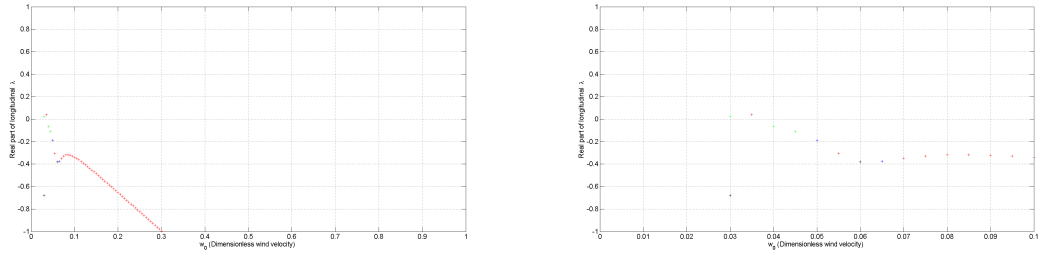

(a) Zoom in (b) Double zoom

Figure 17: Real part of longitudinal eigenvalues zoom

Stand out that 0.04 is a very low value for dimensionless wind velocity. In order to know if this solution is physical or not figure 15 must be analysed. In that figure, it is observable that for this value of wind, the corresponding angle of attack is so much greater than the stall angle, so this solution is not physical and the stability boundary must be defined by lateral variables.

By looking to both figures 16(a) and 16(b) longitudinal modes can be differentiated. It is observable in real part that there are two eigenvalues with same value and two more with different values. Notice that eigenvalues with same real part has same imaginary one but opposite sign; the other

two has zero imaginary part except on at very low values of wind. Notice that at dimensionless wind velocity equals to 0.62, modes change from 3 to 4 where all of them are real.

An analysis for a fixed value of wind in the stable region has been performed. The chosen value is 10m/s whose dimensionless value is 0.2258; a value of 30% greater than the stability limit. Fixing this value Jacobian is calculated by using the following formula at which dh is equal to 10^{-3}:

$$\frac{\partial f_i}{\partial x_i} \approx \frac{f_i(x_1, x_2, ..., (x_i + dh/2), ..., x_n) - f_i(x_1, x_2, ..., (x_i - dh/2), ..., x_n)}{dh} \tag{54}$$

Longitudinal Jacobian after applying equations 51, 52 and 54 is obtained, reading:

$$\boldsymbol{J_{Lon}} = \begin{bmatrix} 0 & 0 & 1 & 0 \\ 0 & 0 & 0 & 1 \\ 1104 & -373 & 1678 & -4963 \\ 421 & -142 & 641 & -1894 \end{bmatrix} \tag{55}$$

Eigenvalue problem is applied to that matrix and eigenvalues-vectors are obtained:

$$\begin{aligned} \lambda_1 &= -66.6228 + 84.6977i \\ \lambda_2 &= -66.6228 - 84.6977i \\ \lambda_3 &= -0.7415 \\ \lambda_4 &= -13.1363 \end{aligned} \tag{56}$$

	$\boldsymbol{v_1}$	$\boldsymbol{v_2}$	$\boldsymbol{v_3}$	$\boldsymbol{v_4}$
$\boldsymbol{\gamma}$	0.0001 + 0.0001i	0.0001 - 0.0001i	-0.8005	-0.0037
$\boldsymbol{\theta}$	-0.0057 - 0.0073i	-0.0057 + 0.0073i	-0.0662	-0.0758
$\boldsymbol{\dot{\gamma}}$	-0.0090	-0.0090	0.5936	0.0480
$\boldsymbol{\dot{\theta}}$	0.9999	0.9999	0.0491	0.9960

Table 4: Longitudinal Eigenvectors

By looking to eigenvalues, the three modes can be seen as introduced before. These modes have been defined as Longitudinal Mode 1 (λ_1 and λ_2), Longitudinal Mode 2 (λ_3) and Longitudinal Mode 3 (λ_4). Some parameters had allowed to characterize the different modes are the time necessary for the excitation to be reduced to the half ($t_{1/2}$), the oscillatory period (T), the natural frequency of the mode, frequency at which the system will oscillate if there were not damping force (ω_n) and the damping ratio, which describe how the oscillations in a system decay after a disturbance (ζ). For finding these parameters the form of the eigenvalue must be: $\lambda = n \pm \omega i$. The parameters are calculated by the following formulas:

$$\begin{aligned} t_{1/2} &= -\frac{0.693}{n} \\ T &= \frac{2\pi}{\omega} \\ \omega_n &= \sqrt{n^2 + \omega^2} \\ \zeta &= -n/\sqrt{n^2 + \omega^2} \end{aligned} \tag{57}$$

For analysing all modes, the equilibrium is perturbed by exciting each mode. This is made by using the eigenvector as a perturbation. A factor ϵ multiply the perturbation for it not to be so higher, with the purpose of being near equilibrium. Different variables in the mode have been analysed along time. The evolution of motion along time ($x_1(\tau)$) reads:

$$x_1(\tau) = \sum c_j x_0 e^{\lambda_j \tau} v_j \tag{58}$$

Where c_j by x_0 is the initial condition, being x_0 equal to the equilibrium point (x^*) plus factor ϵ by the real part of the eigenvalue (v_j).

4.2.2.1 Longitudinal Mode 1

Mode 1 is the mode related to eigenvalues $\lambda_{1,2} = -66.6228 \pm 84.6977i$ and associated eigenvectors are $v_{1,2} = [0.0001 \pm 0.0001i \ -0.0057 \pm 0.0073i \ -0.0090 \ 0.9999]^T$. For these eigenvalues n is equal to -66.6228 and ω is 84.6977. According to that:

$$\begin{aligned} t_{1/2} &= 0.0104 \\ T &= 0.07418 \\ \omega_n &= 107.76 \\ \zeta &= 0.618 \end{aligned} \tag{59}$$

Recall that values obtained from equations 57 are dimensionless, so, for obtaining the values in seconds for time quantities, the dimensionless value must be multiplied by characteristic time t^*. According to that, system needs 0.047 seconds for reducing the excitation to the half, being the quickest mode. The damping ratio indicates that this mode is underdamped, which means that the solution is a decaying exponential combined with an oscillatory portion. The negative real part of the eigenvalue makes the motion after perturbation to be stable, system approach equilibrium and it makes it in an oscillatory motion due to the complex form of the eigenvalue. By looking to figure 18, it is clearly observable that polar diagram is dominated by $\dot{\theta}$; this issue makes the kite to move after perturbation is applied.

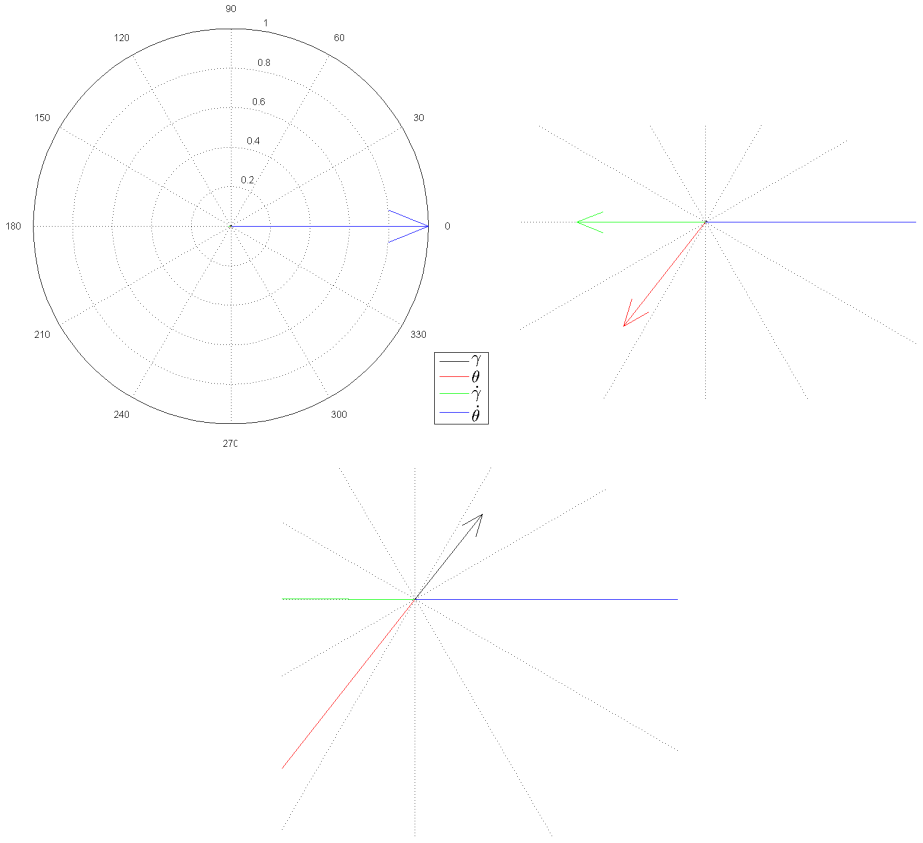

Figure 18: Polar diagram of the longitudinal response against an excitation in the Longitudinal Mode 1 (Zoom out at left side, zoom in at right one and double zoom at bottom)

Via looking to the polar zoom, it is observable that variables are in anti-phase form, the phase between variables is 180º; this means that when $\dot{\theta}$ gets bigger, $\dot{\gamma}$ is reduced. On the other hand, by looking to figure 19, the evolution along time of longitudinal variables can be observed. For this analysis, the value used for ϵ is 10^{-2}. The issue of that is the fastest mode is reaffirmed; equilibrium is reached in less than 0.2 seconds. It is difficult to see, because of the speed of the mode, but the motion to approach equilibrium is oscillatory, as the complex nature of the eigenvalue means. Recall that the symmetric equilibrium point consists on lateral variables equal to zero and longitudinal ones with some value. Values for variables are γ equals to 19.758 degrees and θ equals to -12.837 degrees. Angular velocities are equal to zero in equilibrium, as plots also show.

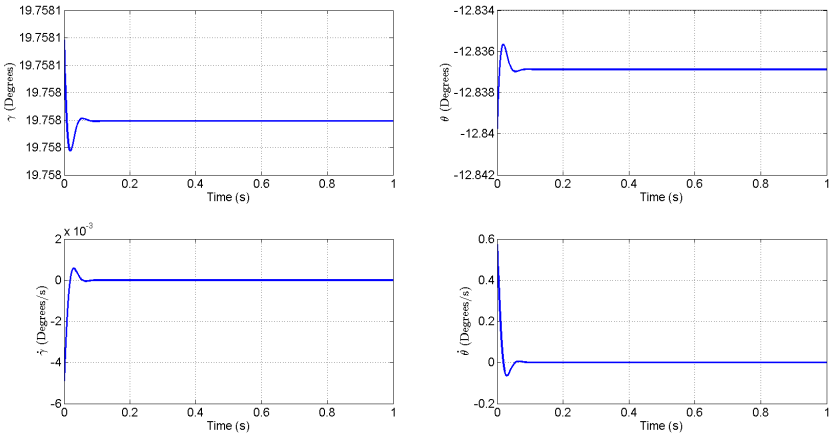

Figure 19: Behaviour of longitudinal variables along time after a perturbation in Longitudinal Mode 1

4.2.2.2 Longitudinal Mode 2

Mode 2 is the mode related to the eigenvalue $\lambda_3 = -0.7415$ and eigenvector $v_3 = [-0.8005 \; -0.0662 \; 0.5936 \; 0.0491]^T$. For this eigenvalue n is equal to -0.7415 and ω is zero. According to that:

$$\begin{aligned} t_{1/2} &= 0.9346 \\ T \; &does \; not \; exist \\ \omega_n &= 0.7415 \\ \zeta &= 1 \end{aligned} \tag{60}$$

The system needs 4.2199 seconds for reducing the excitation to the half, being the slowest mode. The damping ratio indicates that this mode is the critical case, it is critically damped; the motion for approaching equilibrium point is linear, as there are no period and $\zeta = 1$. In the polar diagram can be seen that the longitudinal variables are excited without existing any phase. The more excited variable is γ so motion after perturbation is mainly done by wires.

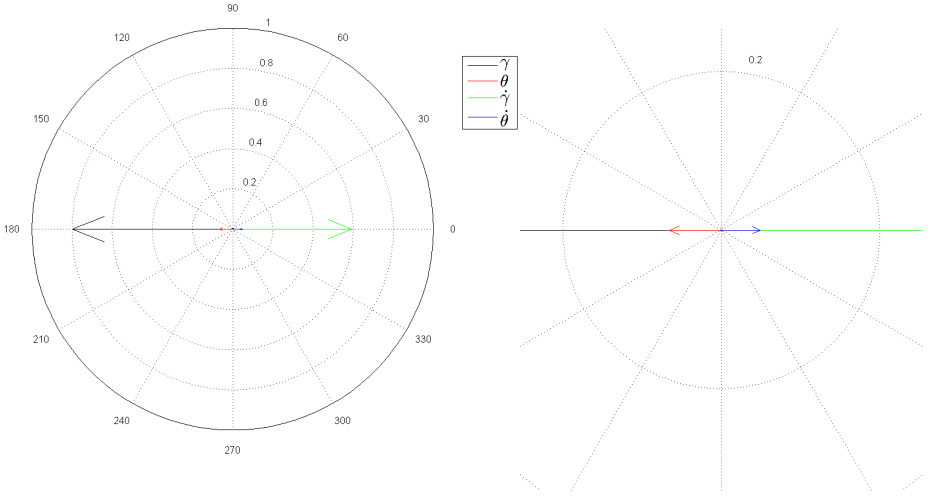

Figure 20: Polar diagram of the longitudinal response against an excitation in the Longitudinal Mode 2 (Zoom out at left side and zoom in at right one)

This mode is the slowest one, it can be seen by looking to $t_{1/2}$ parameter and also by observing figure 21 where it can be realized that equilibrium is reached in more or less 10 seconds. These plots are drawn after a perturbation using a ϵ factor equals to 10^{-1}. Plots also confirm that approach to equilibrium is linear. As in Longitudinal Mode 1, values for γ and θ are reached; and also angular velocities equals to 0.

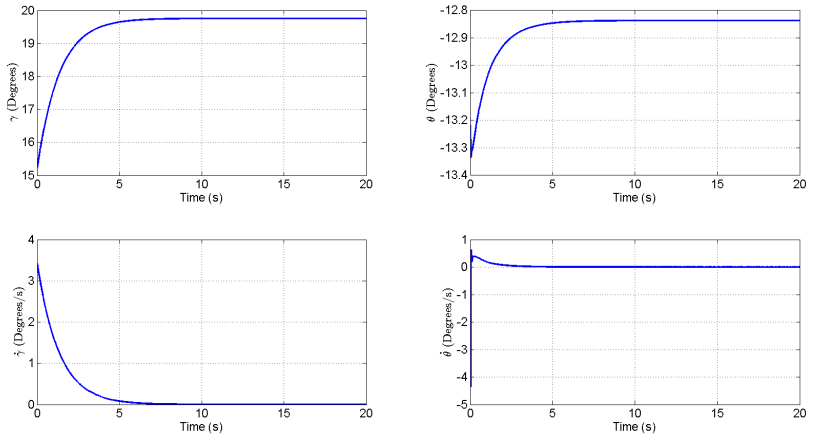

Figure 21: Behaviour of longitudinal variables along time after a perturbation in Longitudinal Mode 2

4.2.2.3 Longitudinal Mode 3

Mode 3 is the mode related to the eigenvalue $\lambda_4 = -13.1363$ and eigenvector $v_4 = [-0.0037 \; -0.0758 \; 0.0480 \; 0.9960]^T$. For this eigenvalue n is equal to -13.1363 and ω is zero. According to that:

$$\begin{aligned} t_{1/2} &= 0.0527 \\ T \; &does \; not \; exist \\ \omega_n &= 13.1363 \\ \zeta &= 1 \end{aligned} \tag{61}$$

The system needs 0.2380 seconds for reducing the excitation to the half. The damping ratio and the absence of period allow to know that approach is linear. Looking to the polar diagram, it is clearly seen that the more excited component is $\dot{\theta}$, so motion after perturbation is made by kite. Longitudinal parameters have zero phase, meaning that both parameters increase together.

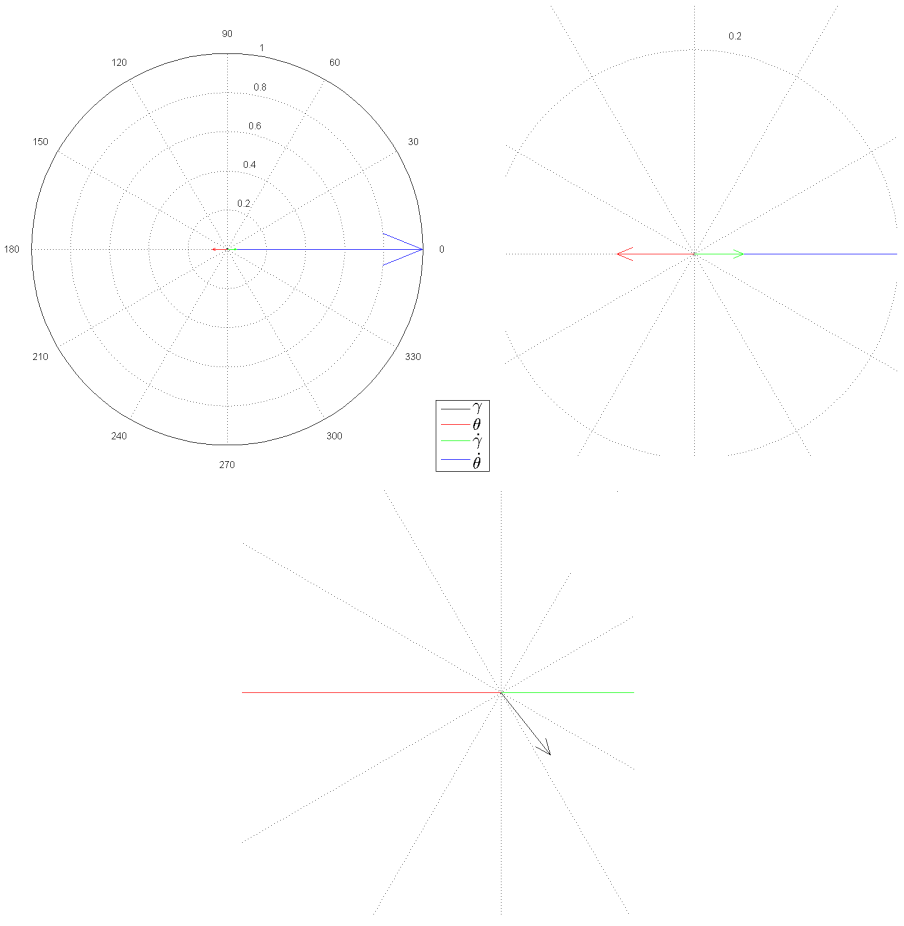

Figure 22: Polar diagram of the longitudinal response against an excitation in the Longitudinal Mode 3 (Zoom out at left side, zoom in at right one and double zoom at bottom)

This mode is fast because it takes less than 1 second to reach the equilibrium linearly as figure 23 shows. For this plots, the chosen value of ϵ is 10^{-2}. Desired values for γ and θ are reached; and also zero angular velocities are encountered.

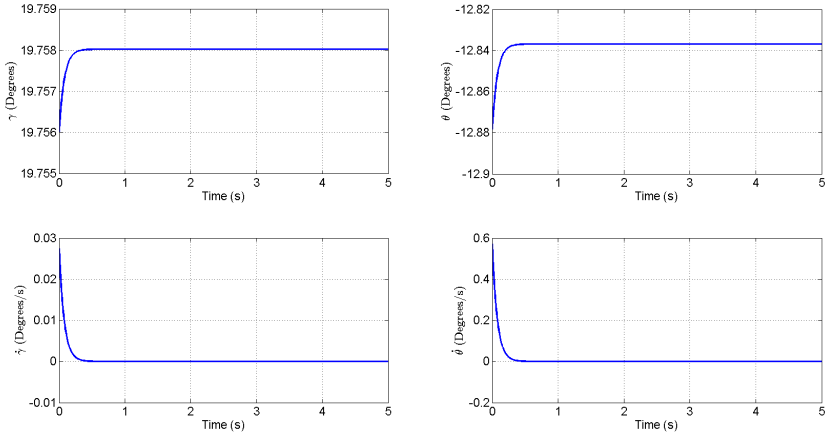

Figure 23: Behaviour of longitudinal variables along time after a perturbation in Longitudinal Mode 3

4.2.3 Lateral stability analysis

In previous section, longitudinal eigenvalues plot (figure 16(a)) showed in its zoom that all real parts of longitudinal eigenvalues became negative at low wind velocities. At that wind velocity, the angle of attack is so much higher than the stall one, so this option as stability boundary was declared inconsistent due to it was not physical. By looking again to figure 15 it can be realized that stability limit was established at dimensionless velocity equal to 0.17 (7.53 m/s in dimension form). As longitudinal eigenvalues did not set up this boundary, it is obvious that this limit is fixed by lateral eigenvalues. For confirming that issue, eigenvalues versus wind velocity graph, figure 24(a), must be analysed.

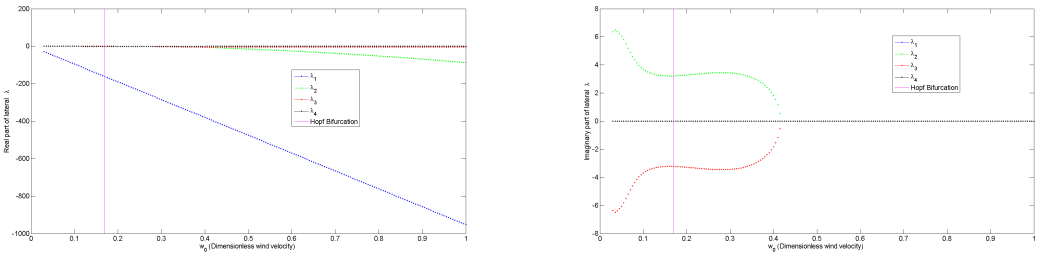

(a) Real part of longitudinal eigenvalues

(b) Imaginary part of longitudinal eigenvalues

Figure 24: Lateral eigenvalues, both real and imaginary parts separately, versus dimensionlesss wind velocity

Zoom should be done to exactly analyse the point at which all eigenvalues are definitely negative. At figure 25(a) an estimation can be performed, but a more zoomed image (figure 25(b)) is needed for accurately determine the value of the stability boundary equal to 0.17 as previous figure 15 presented.

This solution is now physically consistent as its corresponding angle of attack is lower than stall one, corresponding to data presented in figure 15. This means that kite at low velocities is laterally

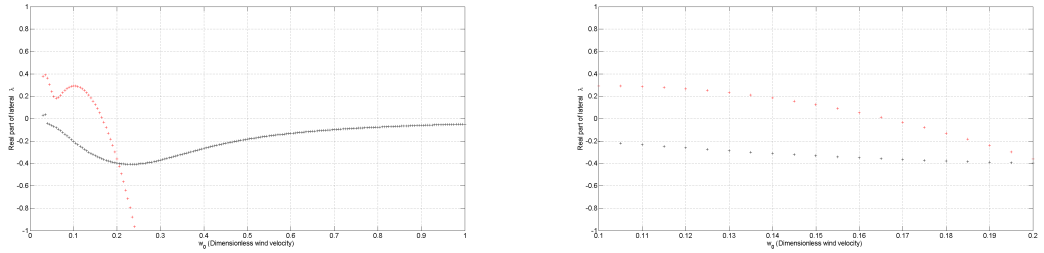

(a) Zoom in (b) Double zoom

Figure 25: Real part of lateral eigenvalues zoom

unstable. In the other hand, by looking to figures 24(a) and 24(b), lateral modes can be differentiated in two modes with only real part and another mode with real and complex part, until dimensionless wind velocity value equals to 0.42 where the kite continues being stable, but modes change into 4 real modes.

As did in longitudinal case, an analysis for fixed wind velocity, 10m/s, is performed. Equation 54 must be also followed for calculating lateral Jacobian matrix. This matrix reads:

$$\boldsymbol{J_{Lat}} = \begin{bmatrix} 0 & 0 & 1 & 0 \\ 0 & 0 & 0 & 1 \\ 76 & 106 & 113 & 2 \\ -9507 & -11724 & -14106 & -261 \end{bmatrix} \tag{62}$$

Eigenvalue problem is again accomplished, in this case for lateral analysis, and the following results are obtained:

$$\begin{aligned} \lambda_1 &= -214.68 \\ \lambda_2 &= -0.73 + 3.35i \\ \lambda_3 &= -0.73 - 3.35i \\ \lambda_4 &= -0.41 \end{aligned} \tag{63}$$

	v_1	v_2	v_3	v_4
φ	0.0044	-0.0564 - 0.2596i	-0.0564 + 0.2596i	0.8975
η	0.0017	-0.0333 - 0.0817i	-0.0333 + 0.0817i	-0.2284
$\dot{\varphi}$	-0.9346	0.9111	0.9111	-0.3657
$\dot{\eta}$	-0.3555	0.2981 - 0.0522i	0.2981 + 0.0522i	0.0931

Table 5: Lateral Eigenvectors

Eigenvalues are again written in form $\lambda = n \pm \omega i$ for calculating parameters introduced in equation 57. These parameters allow to describe in detail the three lateral modes. These modes are Lateral Mode 1, which corresponds to λ_1; Lateral Mode 2, matched to eigenvalue pair λ_2 and λ_3; and Lateral Mode 3, which its associated eigenvalue is λ_4.

4.2.3.1 Lateral Mode 1

Lateral Mode 1 is the mode related to the eigenvalue $\lambda_1 = -214.683$ and eigenvector $v_1 = [0.0044\ 0.0017\ -0.9346\ -0.3555]^T$. For this eigenvalue n is equal to -214.68 and ω is zero. According to that:

$$\begin{aligned} t_{1/2} &= 0.00323 \\ T\ &does\ not\ exist \\ \omega_n &= 214.68 \\ \zeta &= 1 \end{aligned} \tag{64}$$

The system needs 0.0146 seconds for reducing the excitation to the half; this is the fastest mode. Its damping ratio and the absence of period and imaginary part, mean that the approach to equilibrium is linear. In this lateral mode, $\dot{\varphi}$ and $\dot{\eta}$ are the most excited variables, and they are excited without any phase between they, so, as one of them increases, the other one does the same. As both variables are excited, motion after perturbation is performed by both kite and wires.

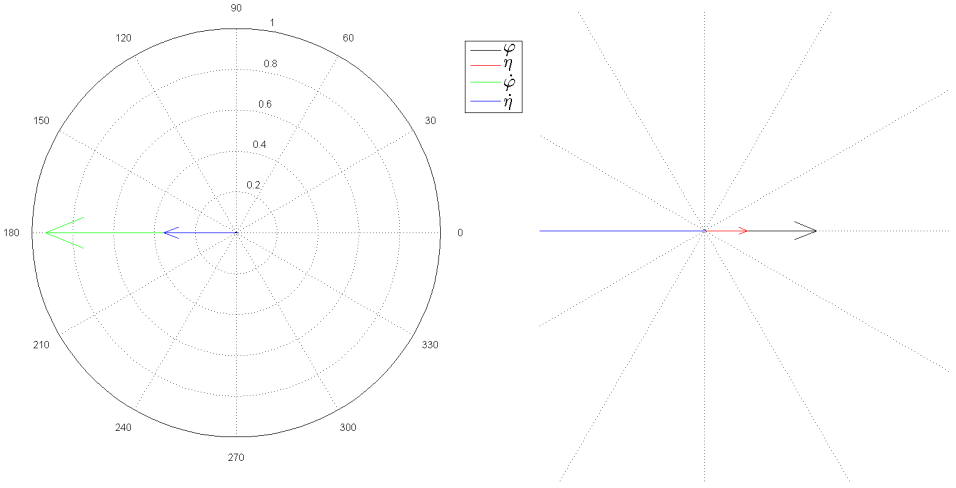

Figure 26: Polar diagram of the lateral response against an excitation in the Lateral Mode 1 (Zoom out at left side and zoom in at right one)

Figure 27 comes out after a perturbation of ϵ equals to 10^{-2}. It shows that equilibrium is reached linearly in less than 0.2 seconds. The values for these lateral variables are zero, as explain before with the concept of symmetric equilibrium, the same than angular velocities.

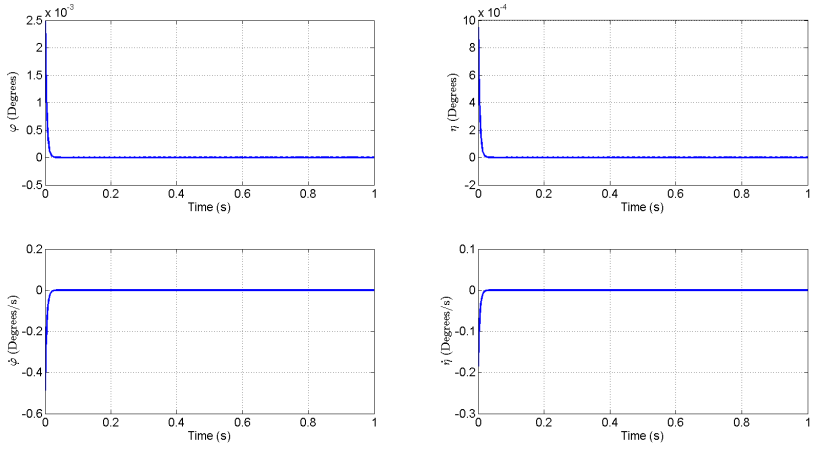

Figure 27: Behaviour of lateral variables along time after a perturbation in Lateral Mode 1

4.2.3.2 lateral Mode 2

lateral Mode 2 is the mode related to eigenvalues $\lambda_{2,3} = -0.73 \pm 3.35i$ and eigenvector $v_{2,3} = [-0.0564 \pm 0.2596i \ -0.0333 \pm 0.0817i \ 0.9111 \ 0.2981 \pm 0.0522i]^T$. For this eigenvalue n is equal to -0.73 and ω is 3.35. According to that:

$$\begin{aligned} t_{1/2} &= 0.9493 \\ T &= 1.8756s \\ \omega_n &= 3.4286 \\ \zeta &= 0.2129 \end{aligned} \tag{65}$$

The system needs 4.2863 seconds for reducing the excitation to the half. The damping ratio indicates that this mode is underdamped, the motion is oscillatory for approaching equilibrium. This mode is dominated by $\dot{\varphi}$ but with a significant contribution of η, with a phase between them of 10 degrees more or less. The contribution of both makes the motion after perturbation to be done by both kite and wires.

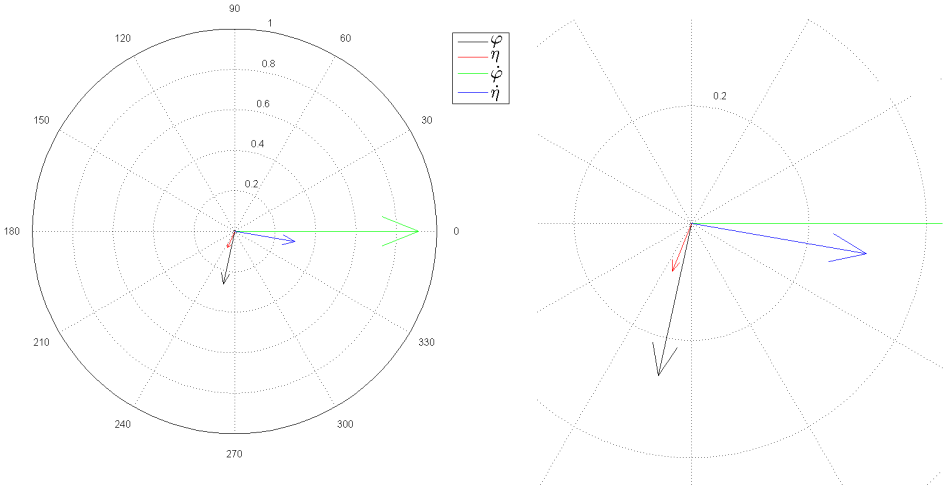

Figure 28: Polar diagram of the lateral response against an excitation in the Lateral Mode 2 (Zoom out at left side and zoom in at right one)

Figure 29 allows to see the oscillatory nature of the mode after a perturbation of ϵ equals to 10^{-2}. Equilibrium, all variables and angular velocities equal to zero, is reached in more or less 10 seconds.

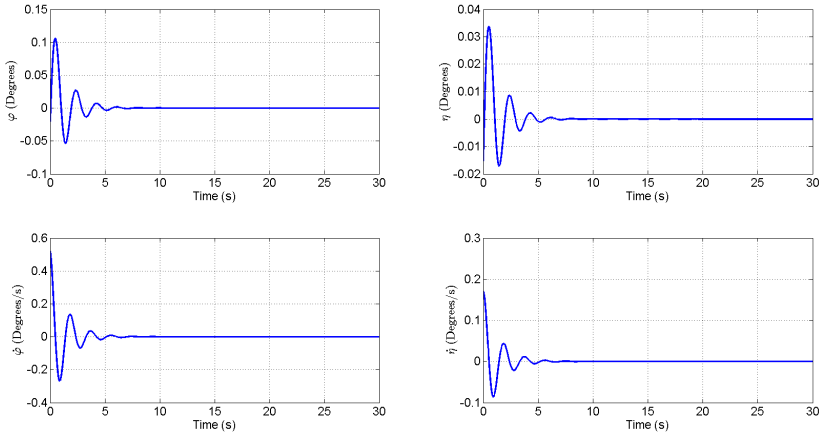

Figure 29: Behaviour of lateral variables along time after a perturbation in Lateral Mode 2

4.2.3.3 Lateral Mode 3

Rolling convergence mode is the mode related to eigenvalues $\lambda_4 = -0.41 \pm 3.35i$ and eigenvector $v_{2,3} = [0.8975 \ -0.2284 \ -0.3657 \ 0.0931]^T$. For this eigenvalue n is equal to -0.41 and ω is zero. According to that:

$$\begin{aligned} t_{1/2} &= 1.69 \\ T \ &does \ not \ exist \\ \omega_n &= 0.41 \\ \zeta &= 1 \end{aligned} \tag{66}$$

The system needs 7.6307 seconds for reducing the excitation to the half, so it is the slowest mode. Again, as Lateral Mode 1, the absence of imaginary part in the eigenvalue, the absence of period and the value of damping ratio show that approach to equilibrium is linear. This mode is characterised by the anti-phase, or 180 degrees phase, of the lateral variables. Polar diagram 30 shows that, mainly, motion is governed by φ but with a contribution not negligible of η, meaning that motion right after the perturbation is done by wires principally, and also by kite in a lesser extent.

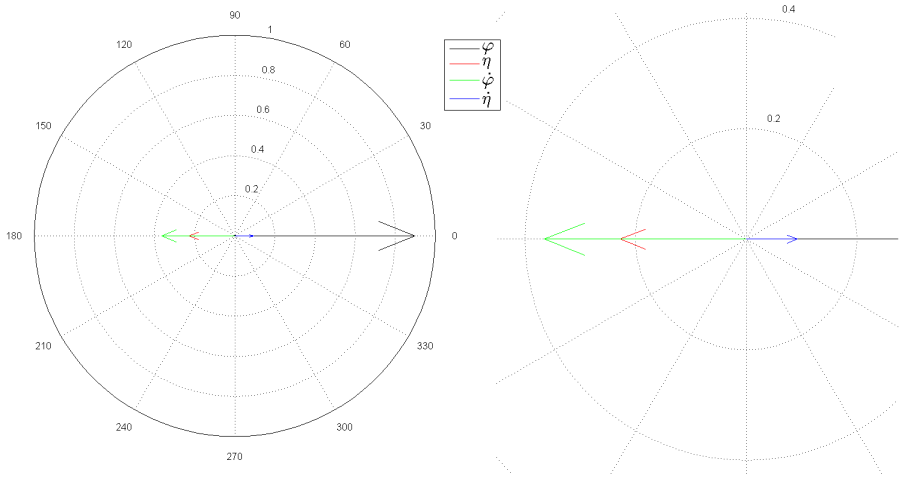

Figure 30: Polar diagram of the lateral response against an excitation in the Lateral Mode 3 (Zoom out at left side and zoom in at right one)

By applying a perturbation of ϵ equals to 10^{-2}, figure 31 draws the evolution of lateral variables confirming that this is the slowest mode, reaching the equilibrium in more or less 17 seconds after a linear motion.

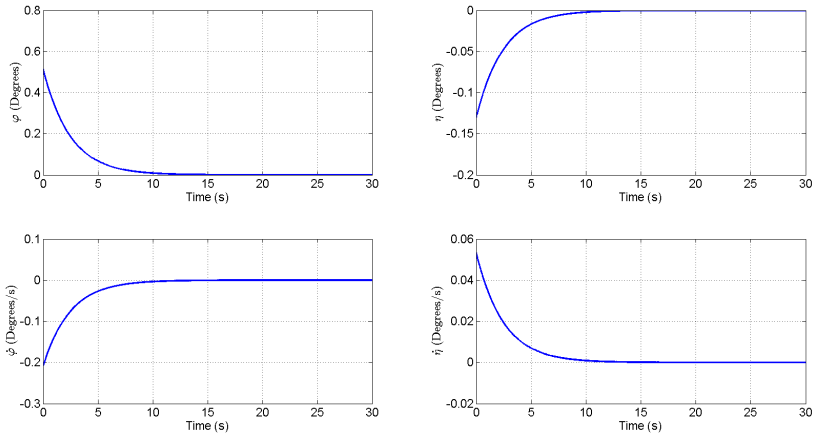

Figure 31: Behaviour of lateral variables along time after a perturbation in Lateral Mode 3

4.3 Non-linear kite dynamics

4.3.1 Kite trajectories close to equilibrium

Kite equilibrium stability is also studied by the non-linear analysis. For that analysis, equations of motion are integrated by *ode45* function in *Matlab* with the initial condition of a perturbed position near equilibrium position x^*; being the perturbation a random quantity of the order 10^{-4}. This random perturbation excites all modes explained before and integrations are done according this issue; in previous integrations, only one mode were excited for each case. Equations are integrated along time and the evolution of state vector along time is analysed.

For this analysis, a value of wind in the stable region is chosen. The value repeats the one selected for eigenvalue problem analysis, 10 m/s. In the stable region, the expected motion of kite after a perturbation is to stabilize the kite by motion of kite and/or wires. In equilibrium, angular velocities must be equal to zero, as well as lateral variables; and longitudinal components, γ and θ must have some value, which is in this case (for this wind) γ = 19.758 degrees and θ = -12.837 as explained in section 4.2.2.1.

As looked for, it can be seen at figure 32 that longitudinal variables reach the desired value and lateral ones converge into zero.

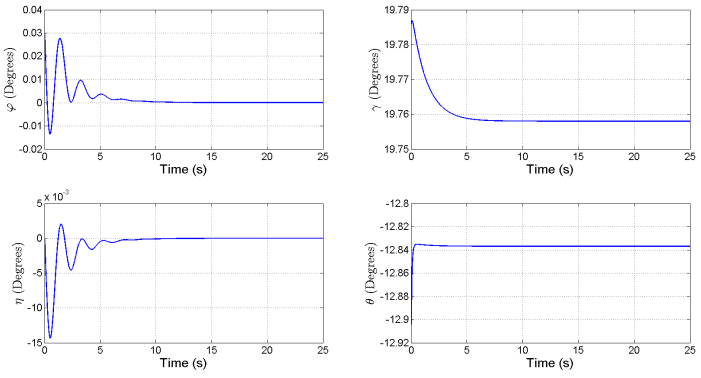

Figure 32: Behaviour of state vector components along time

In the other hand, figure 33 shows how angular velocities, or state vector derivatives, reach 0 value for achieving equilibrium conditions.

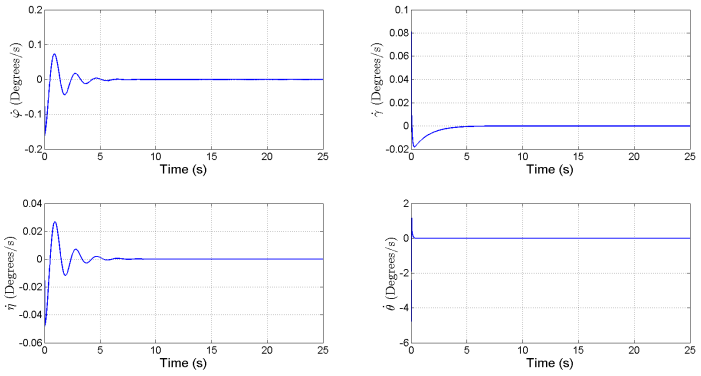

Figure 33: Behaviour of state vector components derivatives along time

By looking to both figures, it is observable that state vector derivatives are the first variables that converge into equilibrium zero value, they spend a little bit less than 10 seconds, except on $\dot{\theta}$ which reaches zero value in more or less 1 second. In case of state vector variables, equilibrium is reached in more or less 15 seconds, again, except on θ component which reaches equilibrium value in 6 seconds.

All variables oscillate after perturbation, clearly observable in lateral components, and visible in longitudinal components thanks to the peaks that can be seen in plots at a low time. This oscillation in both longitudinal and lateral variables is due to the presence of a complex eigenvalue (or which results in an oscillatory motion) at this wind value. In case of longitudinal variables, the mode that affects for motion to be oscillatory is the Longitudinal Mode 1, which is very quick, and that is the reason for not to be a clearly visible oscillation in figures 32 and 33. On the other hand, in case of lateral variables, they move in a more visible oscillatory way thanks to Lateral Mode 2, which is slower than Longitudinal Mode 1 and allows to view oscillations when lateral variables are converging.

4.3.2 Natural periodic orbits

When kite is flying inside the unstable region, motion must be studied with the purpose of looking for new kind of kite behaviour. The instability of the equilibrium position can lead, after a perturbation on kite, into periodic orbits or chaos. A periodic orbit consist on an orbit around kite moves constantly following a determined path; and chaos is a non-regular motion of the system.

An analysis has been performed in the unstable region, specifically at dimensionless wind velocity equals to 0.1 (4.43 m/s) where longitudinal eigenvalues exhibit a negative real part, being stable and physically consistent according to figure 15 where a value for the angle of attack is obtained lower than the stall one; but at this velocity, lateral eigenvalues still be positive in their real parts, causing the instability.

At figure 34 it is observable that the motion begins near equilibrium an it moves away progressively until a periodic orbit is reached with constant period and amplitude. For lateral variables φ and η motion is symmetric and it begin to increase its amplitude at 10 seconds until 28 seconds where there is a peak. After that instant, amplitude stabilizes itself reaching the periodic orbit values at 42 seconds more or less where the amplitude is 75 degrees for φ and 30 for η; the period for both variables is 2 seconds. On the other hand, longitudinal variables take 15 seconds for beginning to increase its amplitude of motion in a non-symmetric behaviour. At 27 seconds it exists a peak and the motion is stabilized after 50 seconds from the initial perturbation acquiring a period of

1 second, which means that longitudinal variables oscillate quicker than lateral ones, and with an amplitude of 21 degrees for γ and 3 degrees for θ.

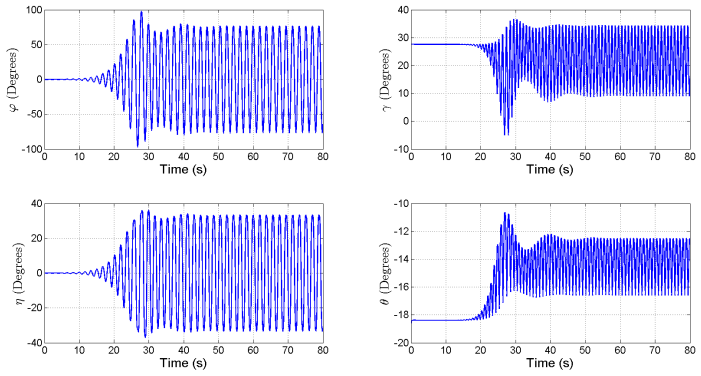

Figure 34: Behaviour of state vector components along time

In case of angular velocities, or state vector derivatives, behaviour along time is symmetric as well as lateral state vector variables with 0 as axis of symmetry, the value that they must acquire in equilibrium, as visible in figure 35. Lateral angular velocities has same behaviour in terms of stabilizing than lateral variables, they have a peak at 28 seconds and the periodic orbit is reached at 42 seconds. In case of longitudinal, times also repeat the ones introduced for state vector variables. Periods are also repeated, 2 seconds for lateral and 1 for longitudinal. Amplitudes are 300 degrees for $\dot{\varphi}$, 175 for $\dot{\eta}$, 75 for $\dot{\gamma}$ and 15 for $\dot{\theta}$.

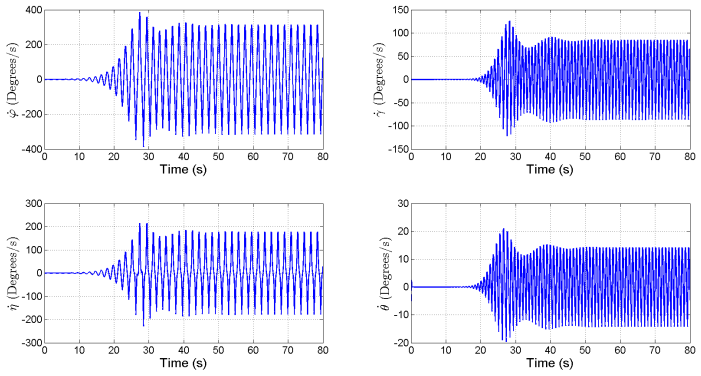

Figure 35: Behaviour of state vector components along time

Recall that this instability lead into a periodic orbit which can be seen in all plots explained, but it is easier to see in space by representing the 3D phase space of γ, θ and η. It can be observable in figure 36 where the motion is drawn from the equilibrium which motion departs near of it.

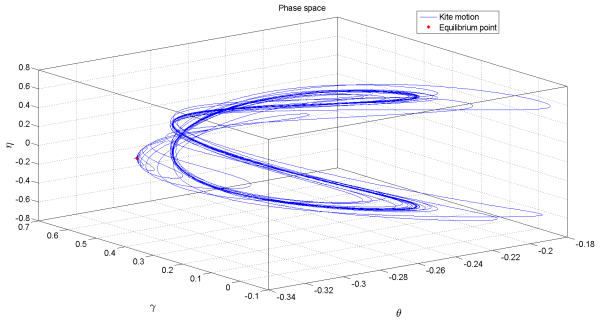

Figure 36: Periodic orbit

5 Planning and Project budget

Before beginning this Bachelor Thesis, a plan was done taking into account the maximum number of weeks available. As can be seen in Gantt diagram of figure 37, the plan predicted (green squares) to make tasks one after the previous, but in actual thesis procedure, some tasks was underhand (actual process in orange, mixing colors in squares that coincide both). Kite modelling was started during the last week of bibliography research because of the information about the complexity of finding a proper model.

Equilibria computation was delayed by 1 week, but it was balanced thanks to the stability analysis which was ended quicker than predicted. Same issue affected the computation of periodic orbit, allowing to start the review of results before planned date and it took 1 week more after the planned end in order to confirm that all results are correct, coinciding 2 weeks with the process of writing the thesis or report which was started 1 week before projected date for dedicating more time to structure and properly writing it. The presentation of the thesis was done in the predicted date and duration.

An average of 3 hours a day, assuming 5 days work in a week, lead into a total of 480 working hours for completing this Bachelor Thesis which is equivalent to 12 ECTS. An ECTS is defined by a work of 25-30 hours, obtaining a maximum total of 360 hours. This thesis was completed in more than this hours because of its investigation nature.

A budget was performed for this thesis assuming working hours, needed licenses, electricity and utilized devices. Unitary costs are collected in table 6 and total costs are shown in table 7.

Working cost	20 €/h
Matlab Academic License	500 €
Electricity cost	0.121 €/h
Laptop	800 €

Table 6: Unitary costs

Total working cost	9600 €
One *Matlab* Academic License	500 €
Total electricity cost	58.08 €
One laptop	800 €
Total cost	10958.08 €

Table 7: Total costs

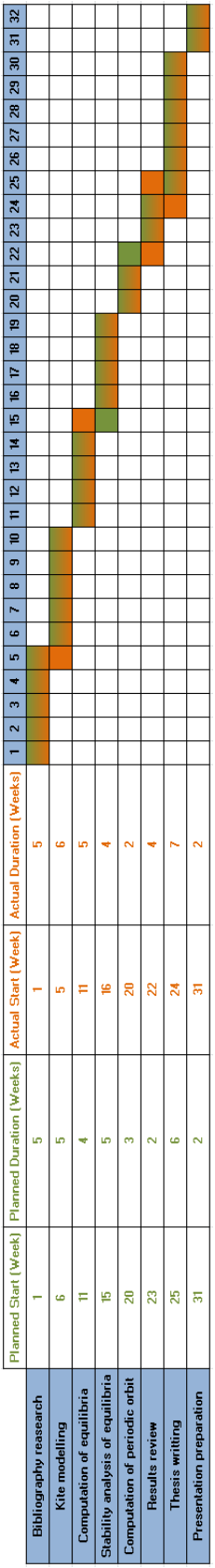

Figure 37: Gantt diagram for planning

6 Conclusions and future works

6.1 Conclusions

This two-lines kite updates the previous models used for energy generation and propulsion of vehicles. For those purposes, control is necessary at kite, [5] used flanges to command the kite and two-lines in present model make this job. In present Bachelor Thesis, control is not applied, so system is time independent.

Dimensionless quantities are used for all calculations in this Bachelor Thesis. In Preliminary background section, dimensionless time is introduced and it plays an important role for all derivations. This section also describes the geometry of the kite, which is assumed a rigid body, deformations and flexibility are not considered for this model. Kite has two planes of symmetry and in the cross-section plane of kite, its shape is elliptic. By knowing the geometry and the property of constant mass distribution, center of mass of kite could be easily founded. This point is important to know for placing kite in space and by knowing its position, attached points can be located; they are the points at which both wires are joined to kite. The other ends of both wires are connected to the ground station which let control kite, but not utilized in this Thesis. This ground station is equivalent to the origin of Earth frame, respect to that velocity of center of mass should be represented.

From the relation of Earth frame and Body frame (the one placed with origin at kite center of mass) appears the state vector, a vector composed by four angles corresponding to the rotations done for changing from Earth to Body frames and also to the number of degrees of freedom of the system (6 dof of a rigid body minus 2 constraints, both tethers). Control vector, a time dependent one, appears also naturally when applying rotations; it is composed by two variables which are the length of the triangle median formed by wires and line between attached points, and angle δ, an angle between this line and z_2-axis.

Angular velocities that appear thanks to rotations, position vector, and linear velocity of center of mass, expressed in matrix form, are written in terms of both vectors. Linear acceleration is not needed due to the use of analytic mechanics which only needs velocities for reaching differential equations with absence of ligatures which classical mechanics utilizes. The formulation which write these differential equations following this analytic mechanics is the Lagrangian formulation. It constructs differential equations of second order from kinetic and potential energies which use velocities and position vector, respectively, and generalized forces, composed by derived velocities and aerodynamic forces and moments, built up in the aerodynamic model. Obtained four equations are transformed in eight by expanding the state vector.

The principal purpose of this Bachelor Thesis is to find equilibrium positions and study them. Symmetric equilibrium is analysed, implying that lateral variables are zero in equilibrium. This condition, together with some more which pass through the evidence that, at equilibrium, state vector derivatives (angular velocities) must be zero, lead into 2 non-trivial equations to solve by Newton's method.

With equilibrium position setted up, its stability must be studied. For that purpose, the application of a perturbation is necessary. The obtained equation is linearised and a Jacobian matrix becomes under study. This matrix transforms the problem into an eigenvalue one for studying stability. Near equilibrium, Jacobian matrix is disengaged separating lateral Jacobian matrix from longitudinal one. Longitudinal and lateral stabilities should be studied separately and put them in common to find a stability boundary in terms of wind velocity, the only parameter that can change in search of symmetric equilibrium. Real part of eigenvalues allows to know if equilibrium is stable or not. Stability boundary establishes a bifurcation called Hopf bifurcation.

This bifurcation suppose the frontier between unstable and stable regions; for low wind the system is unstable. An analysis in the stable region for fixed wind was performed to determine the different modes of kite. These modes can be previously predicted by plotting the real (this plot clarify that longitudinal eigenvalues become stable at low wind values, physically inconsistent because of this wind value means an angle of attack so much higher than stall one) and imaginary part separately versus wind velocity.

In the longitudinal analysis it can be realized that there are 3 modes, two real ones and a complex mode which is very fast. Real part of eigenvalue of each mode let know how fast the mode is; and imaginary part, if exists, indicate that mode is oscillatory, that equilibrium is reached by an oscillatory motion; in case of absence of imaginary part, approach to equilibrium is linear. Two variables γ and θ are the longitudinal ones, and eigenvector indicates which one has more influence in motion. Influence of γ signify a motion in tether after perturbation exciting the selected mode and if the eigenvector denotes that θ dominates, kite motion occurs after the disturbance. Fastest longitudinal mode is the complex one at which kite motion dominates, as well as in one of real modes; on the other hand, the other real mode, the slowest one, is dominated by tether motion.

For completely analyse modes and confirming the time that they need to recover equilibrium position, the evolution on time of these longitudinal variables and also its derivatives was plotted after a perturbation exciting only each mode. This let confirm and see graphically the behaviour of system with an oscillatory or linear approach, the speed to stabilize and that desired value for angles and angular velocities are reached.

Lateral analysis is performed by following similar procedures used for longitudinal. By real part of eigenvalues versus wind velocity plot, it is observable that stability boundary is established by lateral variables, meaning that for low wind values, system is laterally unstable. This plot together with the imaginary part or eigenvalues versus wind let differentiate 3 modes as in longitudinal analysis. These modes are two real and one complex which in this lateral case is slower. In this case, the meaning of angle influence is that motion is governed by wires if eigenvector denotes a strong role of φ and in other hand, if eigenvector shows a higher influence of η, it indicates that motion is commanded by kite.

Lateral real modes describe an antithesis being one of them very quick and the other one so slow. In both modes motion is governed by tethers but in the fastest one, kite motion is also present. The complex mode describe a motion after perturbation similar in influence to fastest real mode, by being principally governed by wires but with a strong importance of kite motion. Modes are also excited and plotted the evolution of angles and their derivatives along time to analyse the modes as did for longitudinal ones.

Non-linear analysis was also performed to find the evolution of all variables along time after exciting all modes by a random perturbation thanks to *Matlab*. This analysis is carried out not only for stable region with same fixed wind value of previous analysis, but also for unstable region in order to find the evolution of variables when going further equilibrium.

The analysis of the unstable region leads into the fact that a periodic orbit is reached naturally when equilibrium point is unstable and a perturbation is applied. This orbit can be observed in space by the 3D-plot of variables. In this motion, lateral variables has a period higher than longitudinal ones which means that periodic orbit is quicker in its longitudinal components. The conclusion that can be obtained from this stable periodic orbit is that it indicates that Hopf bifurcation is supercritical.

These kind of orbits are the ones looked for with the purpose of energy generation, but they are more efficient when control is introduced.

6.2 Future works

The study of present model can be continued by so many ways. As explained in this Bachelor Thesis, position vector and center of mass velocity are calculated as a function of state and control vectors. Control vector in present thesis is constant because controls are not applied. Time dependent control vector can be implemented for continue the study of this model.

Flexibility effects can be introduced in kite, adding degrees of freedom. In case of tethers, flexibility effects can also be studied and its mass can be taken into account because in present calculations, wires are assumed massless and also is neglected its contribution to aerodynamic drag.

In case of aerodynamic model, it can be improved in order to make the system better for energy generation. Optimum thrust laws can be looked for in order to find an optimum force which maximizes the produced energy.

For equilibrium, at present thesis, only symmetric equilibrium positions were founded. With lateral variables playing a role, breaking the symmetry, more equilibrium position can be computed and the study of their stability can lead into a new periodic orbit which appears naturally because of wind and can produce energy without the need of controlling kite with ground station.

References

[1] The need project. *Solar at a glance.* 2008.

[2] U.S. department of the Interior. *Reclamation. Managing water in the West, Hydroelectric power.* 2005.

[3] Peter McKendry. *Energy production from biomass (part 1): overview of biomass.* 2001.

[4] Dave North. *High Altitude Wind Power.* 2016.

[5] J. Alonso-Pardo and G. Sanchez-Arriaga. *Kite Model with Bridle Control for Wind-Power Generation*, volume 52. 2015.

[6] A.R. Podgaetz and W.J. Ockels. *Robust Control of Laddermill Wind Energy System.* 2007.

[7] Mr. Sankaran Nampoothiri K and Ms. Dhanya G. *A Review on Flying Electric Generator as an Alternate Source of Energy Harvester*, volume 3. 2015.

[8] Dr. Anil Kane. *Presentation 'Can Wind Power Meet The World Electricity Demand'.* 2015.

[9] Lorenzo Fagiano Massimo Canale and Mario Milanese. *Power Kites for Wind Energy Generation.* 2007.

[10] Skysails. *www.skysails.info/english.* 2016.

[11] Björn Allenström. *Wind propulsion.* 2013.

[12] M. Diehl, L. Magni, and G.Nicolao. *Efficient NMPC of unstable periodic systems using approximate infinite closed loop costing*, volume 28. 2004.

[13] Makani. *https://www.google.com/makani/.* 2016.

[14] Makani. *Google X acquires Makani Power for kite-like airborne wind turbines, https://www.youtube.com/watch?v=4CH7qmMid5g.* 2016.

[15] Benjamin E. Isabella Michael R. Blouin Jr. and Joshua E. Rodden. *Wind Power from Kites.* 2007.

[16] Jeroen Breukels. *An Engineering Methodology for Kite Design.* 2010.

[17] Michael Fowler. *Notes on Special Relativity.* 2008.

[18] R. Schmehl G. Sanchez-Arriaga, M. García Villalba. *A two-line kite dynamic model for airborne wind energy generation.*

[19] Bernard Etkin and Lloyd Duff Reid. *Dynamics of flight. Stability and control.* 1996.

[20] WSBCTC. *Newton's method for finding roots.*

[21] Wikipedia. *Hopf bifurcation.* 2016.

[22] Yousef Saad. *Numerical methods for large eigenvalue problems.* Society for Industrial and Applied Mathematics, 2011.